The Astrophysical Journal, 923:44 (31pp), 2021 December 10 https://doi.org/10.3847/1538-4357/ac2954

Identifying Circumgalactic Medium Absorption in QSO Spectra: A Bayesian Approach

Jennifer E. Scott[1], Emileigh S. Shoemaker[1,2], and Colin D. Hamill[1,3]
[1] Department of Physics, Astronomy, and Geosciences, Towson University, 8000 York Road, Towson, MD 21252, USA; jescott@towson.edu
[2] Lunar and Planetary Laboratory, University of Arizona, 1629 East University Boulevard, Tucson, AZ 85721, USA
[3] Department of Earth, Atmospheric and Planetary Sciences, 550 Stadium Mall Drive, Purdue University, West Lafayette, IN 47907, USA
Received 2021 April 26; revised 2021 August 16; accepted 2021 August 23; published 2021 December 9

Abstract

We present a study of candidate galaxy–absorber pairs for 43 low-redshift QSO sightlines ($0.06 < z < 0.85$) observed with the Hubble Space Telescope/Cosmic Origins Spectrograph that lie within the footprint of the Sloan Digital Sky Survey with a statistical approach to match absorbers with galaxies near the QSO lines of sight using only the SDSS Data Release 12 photometric data for the galaxies, including estimates of their redshifts. Our Bayesian methods combine the SDSS photometric information with measured properties of the circumgalactic medium to find the most probable galaxy match, if any, for each absorber in the line-of-sight QSO spectrum. We find ∼630 candidate galaxy–absorber pairs using two different statistics. The methods are able to reproduce pairs reported in the targeted spectroscopic studies upon which we base the statistics at a rate of 72%. The properties of the galaxies comprising the candidate pairs have median redshift, luminosity, and stellar mass, all estimated from the photometric data, $z = 0.13$, $L = 0.1L^*$, and $\log(M_*/M_\odot) = 9.7$. The median impact parameter of the candidate pairs is ∼430 kpc, or ∼3.5 times the galaxy virial radius. The results are broadly consistent with the high Lyα covering fraction out to this radius found in previous studies. This method of matching absorbers and galaxies can be used to prioritize targets for spectroscopic studies, and we present specific examples of promising systems for such follow-up.

Unified Astronomy Thesaurus concepts: Circumgalactic medium (1879); Intergalactic medium (813); Galactic and extragalactic astronomy (563)

Supporting material: machine-readable tables

1. Introduction

Since the discovery of QSO absorption lines, their origin in both the gaseous material in galaxies and in the truly intervening intergalactic medium (IGM) has been debated (Bahcall & Salpeter 1965; Gunn & Peterson 1965; Bahcall & Spitzer 1969). Statistical studies of QSO absorption lines have long been the primary avenue for characterizing the unvirialized structures in the cosmic web; see reviews by Meiksin (2009) and McQuinn (2016). The connection of the strongest of these absorption features, the damped Lyα systems with $\log N_{\rm H\,I} \gtrsim 20$, to galaxy disks has also long been recognized and leveraged to measure the physical properties of galaxy gas phases at high redshift and their evolution over cosmic time (Wolfe et al. 2005).

Absorption features with lower column densities offer a very effective probe of the diffuse gas in galaxy halos, provided that absorption features can be attributed to a particular galaxy. Early studies of low-redshift galaxy–absorber relationships (Morris et al. 1993; Bowen et al. 1995, 1996, 1997; Lanzetta et al. 1995; Chen et al. 1998, 2001b, 2001a; Tripp et al. 1998; Bowen et al. 2002) established that galaxies over a wide range of luminosity and morphological type possess extended H I halos that can be probed using the line-of-sight spectra of QSOs at impact parameters $\lesssim 200$ kpc. The studies showed that the H I halos have ∼70% covering fractions and extents that scale with galaxy luminosity.

The one-to-one association of absorption features with $\log N_{\rm H\,I} < 14$ with galaxies is more ambiguous (Chen et al. 2005). Statistical studies show associations of galaxies and weaker absorbers to 1 Mpc or more (Morris et al. 1993; Tripp et al. 1998; Tejos et al. 2014), consistent with the positions of galaxies within the large-scale structure of the cosmic web (Prochaska et al. 2011b; Burchett et al. 2020; Wilde et al. 2021).

In the last decade, understanding of the structure of the gaseous halos within the virial radii of galaxies, i.e., the circumgalactic medium or CGM, and its role in the physical relationship between the IGM and galactic processes has expanded, thanks to targeted spectroscopic surveys of QSOs with close projected distances to regular galaxies at low redshift (Wakker & Savage 2009; Tumlinson et al. 2011, 2013; Prochaska et al. 2011b; Stocke et al. 2013; Werk et al. 2013, 2014; Keeney et al. 2017) and high (Rudie et al. 2012, 2013; Turner et al. 2014, 2015; Rudie et al. 2019), or specific populations such as dwarf galaxies (Bordoloi et al. 2014; Borthakur et al. 2016; Johnson et al. 2017), starbursts (Borthakur et al. 2013; Heckman et al. 2017), early type galaxies (Thom et al. 2012), luminous red galaxies (Smailagić et al. 2018; Zahedy et al. 2019), or quasar host galaxies (Johnson et al. 2015). Comparisons with hydrodynamic simulations (Oppenheimer et al. 2018; Nelson et al. 2019; Peeples et al. 2019) enable detailed examinations of the physical interplay between IGM accretion, metal production in stars, and outflows from supernovae.

The results of the targeted studies of the low-redshift CGM, e.g., from the COS-Halos Project, demonstrate the presence of a substantial gas reservoir within ∼300 kpc of galaxies, with an H I covering fraction of nearly 100% for star-forming galaxies and ∼75% for passive galaxies (Tumlinson et al. 2013) to ∼150 kpc and an average covering fraction of 60% out as far as 500 kpc (Liang & Chen 2014). The Keck Baryonic Structure Survey finds galaxy–absorber correlations are particularly tight for high column density absorbers, $\log N({\rm H\,I}) > 14.5$, and present at lower column densities out to scales of 2 Mpc at

$z \sim 2.3$ Rudie et al. (2012). The Lyα covering fraction in this survey is found to be ~80% within ~200 kpc for $\log N(\mathrm{H\,I}) = 15$–17.

A declining CGM metal surface density with increasing distance from galaxies is manifested as a distinct anticorrelation between the equivalent width of absorption features measured along lines of sight at different impact parameters. These relationships were shown in early studies of H I and C IV (Chen et al. 2001a, 2001b), and have now been measured in a variety of other metal line transitions including O VI, N V, Si IV, Si III, C III, and C II, allowing for detailed ionization modeling, indicating a multiphase structure of a hot $T \sim 10^{5.5}$ K corona with smaller, cooler clouds embedded within (Werk et al. 2014, 2016; Burchett et al. 2015; Keeney et al. 2017).

Several observed properties of the CGM indicate the influence of galactic outflows from supernovae. H I is common for sightlines intersecting the halos of both passive and star-forming galaxies, with modest dependence on star formation rate in the sense that the strongest features are typically observed near star-forming galaxies (Tumlinson et al. 2011; Thom et al. 2012; Borthakur et al. 2016). There is a strong association of O VI with galaxies, particularly massive galaxies with high specific star formation rates, $\gtrsim 10^{-11}$ yr^{-1} (Chen & Mulchaey 2009; Prochaska et al. 2011b; Mathes et al. 2014; Werk et al. 2016; Prochaska et al. 2019), extending to ~ 330–350 kpc (Muzahid 2014; Bielby et al. 2019). On the other hand, C IV is estimated to extend to ~100 kpc in galactic halos at both low (Chen et al. 2001a) and high redshift (Steidel et al. 2011). Dwarf galaxies show a similar gaseous extent and a correlation with star formation rate similar to O VI, though weaker than found for more massive galaxies (Bordoloi et al. 2014). In a blind survey of C IV with $z < 0.16$, Burchett et al. (2016) find that C IV absorption is dependent upon both stellar mass and galaxy environment, with high-mass ($M_* > 10^{9.5} M_\odot$) galaxies in low-density environments showing the highest rates. All of these studies lead to the model of an extended warm, metal-enriched CGM bound to galaxies. The general conclusion is that galaxies contain significant reservoirs of H I and metals within ~300 kpc, and that these reservoirs play a key role in the star formation processes within the galaxy (Tumlinson et al. 2017).

Because establishing the physical relationship between specific absorption features and galaxies relies on measuring a coincidence in redshift, the targeted surveys make use of extensive spectroscopic observations of galaxies in QSO fields (Chen & Mulchaey 2009; Prochaska et al. 2011a; Werk et al. 2012; Keeney et al. 2018; Prochaska et al. 2019) or archival data of galaxy redshifts and other properties (Wakker & Savage 2009; Liang & Chen 2014). We define a process by which likely galaxy–absorber pairs may be identified so that these galaxies may be targeted and follow-up spectroscopic observing resources optimally placed—for example, by determining whether fainter galaxies closer to a particular QSO sightline versus brighter galaxies at larger impact parameter may be most likely to result in specific absorption features in the QSO line-of-sight spectrum.

The methods presented here leverage the abundance of photometric data in the Sloan Digital Sky Survey (SDSS), and the ability to use photometry alone to estimate photometric redshifts and other galaxy properties. A photometric redshift alone is not sufficiently accurate to establish galaxy–absorber relationships, but in combination with other measured or estimated galaxy properties such as color, virial radius, and stellar mass; absorber properties such as equivalent width and the presence of metals; and characteristics of the potential galaxy–absorber pair, e.g., impact parameter, we may draw upon the wealth of targeted CGM studies to modify a set of priors and obtain a probability that a particular galaxy and absorber are physically associated with one another. We use this probability to examine trends in the galaxy–absorber pairs versus galaxies within the same impact parameter that are not associated with absorbers. Our approach is similar to Liang & Chen (2014) in that we are mining the SDSS data sets and comparing to QSO spectra from the Cosmic Origins Spectrograph (COS) on the Hubble Space Telescope. However, because we do not require a spectroscopically confirmed galaxy redshift, we have the ability to investigate more possibilities for associations between galaxies near the QSO lines of sight and absorption features in the QSO spectra. In this way, the method compares to photometric redshift surveys of $z < 1$ DLAs and Lyman-limit systems (Chen & Lanzetta 2003; Rao et al. 2011). We compare our results to known galaxy–absorber pairs in our fields as a check on the method.

Throughout this paper, we assume the following values of cosmological parameters: $H_0 = 69.6$, $\Omega_M = 0.286$, and $\Omega_\lambda = 0.714$ (Bennett et al. 2014).

2. Data

Of the 82 QSOs with COS spectra in the sample of Danforth et al. (2016) and archived in the Mikulski Archive for Space Telescopes (MAST), 43 of them, and their surrounding fields, overlap with the footprint of the SDSS. Table 1 lists these QSOs, which constitute our sample. We use the Danforth et al. (2016) absorption linelists downloaded from MAST,[4] with identifications, redshifts, equivalent widths, and significance values for the absorption features in the COS spectra.

We queried the SDSS DR12 database (Alam et al. 2015) to gather all galaxies within three degrees of each QSO sightline. This search radius corresponds to a radius of ~0.16 (83) Mpc for $z = 0.00073$ (0.85) the lowest (highest) redshift absorption lines in the QSO sample. These queries returned u, g, r, i, and z magnitudes of all galaxies with clean photometry and $r > 14$ within the search radius, as well as their photometric redshift and position angle and the Galactic extinction. We corrected galaxy magnitudes for extinction in each band and applied small offsets in u and i to convert to AB magnitudes. For all calculations based on these magnitudes, we use K-corrections from Chilingarian et al. (2010) and Chilingarian & Zolotukhin (2012), and thus restrict our sample to $z_{\mathrm{phot}} < 0.5$, the applicable range for their parameterizations. To generate the final galaxy catalogs for each QSO field, we also filtered the results to include only those with the highest-quality photometric redshifts, SDSS photoErrorClass = 1, and rms = 0.043 (Beck et al. 2016). This limits our ability to treat the lowest-redshift galaxy–absorber pairs with $z \lesssim 0.01$.

The resulting galaxy catalogs for the 43 QSO fields contain ~93K galaxies each. Distributions of the redshifts of the sample QSOs, as well as the SDSS photometric and spectroscopic redshifts where available, of all the galaxies in the SDSS sample are shown in Figure 1, along with the photometric redshifts and SDSS r magnitudes of all sample galaxies. In order to evaluate our methods, we discuss the agreement

[4] MAST DOI: https://doi.org/10.17909/T95P4K.

Table 1
HST/COS QSO Sample in SDSS Footprint

Quasar	Short Name[a]	R.A. (J2000.0)	Decl. (J2000.0)	z_{em}
PG0003+158	pg0003	00:05:59.24	+16:09:49.0	0.4509
PG0026+129	pg0026	00:29:13.71	+13:16:04.0	0.1420
QSO0045+3926	q0045	00:48:18.99	+39:41:11.6	0.1340
PG0157+001	pg0157	01:59:50.25	+00:23:41.3	0.1631
SDSSJ080908.13+461925.6	s080908	08:09:08.14	+46:19:25.7	0.6563
PG0832+251	pg0832	08:35:35.80	+24:59:41.0	0.3298
PG0844+349	pg0844	08:47:42.45	+34:45:04.4	0.0640
MRK106	mrk106	09:19:55.36	+55:21:37.4	0.1230
SDSSJ092554.43+453544	s09255b	09:23:54.43	+45:35:44.3	0.3295
SDSSJ092909.79+464424	s092909	09:29:09.79	+46:44:24.0	0.2400
SDSSJ094952.91+390203	s094952	09:49:52.91	+39:02:03.9	0.3656
PG0953+414	pg0953	09:56:52.41	+41:15:22.1	0.2341
PG1001+291	pg1001	10:04:02.59	+28:55:35.2	0.3297
FBQS1010+3003	f1010	10:10:00.70	+30:03:22.0	0.2558
TON1187	ton1187	10:13:03.20	+35:51:23.0	0.0789
1ES1028+511	1es1028	10:31:18.50	+50:53:36.0	0.3604
1SAXJ1032.3+5051	1sj1032	10:32:16.10	+50:51:20.0	0.1731
PG1048+342	pg1048	10:51:43.90	+33:59:26.7	0.1671
PG1049-005	pg1049	10:51:51.48	-00:51:17.6	0.3599
HS1102+3441	hs1102	11:05:39.80	+34:25:34.4	0.5088
SBS1108+560	sbs1108	11:11:32.20	+55:47:26.0	0.7666
PG1115+407	pg1115	11:18:30.30	+40:25:54.0	0.1546
PG1116+215	pg1116	11:19:08.60	+21:19:18.0	0.1763
PG1121+422	pg1121	11:24:39.18	+42:01:45.0	0.2250
SBS1122+594	sbs1122	11:25:53.79	+59:10:21.6	0.8520
TON580	ton580	11:31:09.50	+31:14:05.0	0.2902
3C263	3c263	11:39:56.99	+65:47:49.2	0.6460
PG1216+069	pg121	12:19:20.93	+06:38:38.5	0.3313
PG1222+216	pg122	12:24:54.40	+21:22:46.0	0.4320
3C273	3c273	12:29:06.70	+02:03:08.7	0.1583
Q1230+0115	q1230	12:30:50.00	+01:15:21.5	0.1170
PG1229+204	pg1229	12:32:03.61	+20:09:29.4	0.0630
PG1259+593	pg1259	13:01:12.90	+59:02:07.0	0.4778
PG1307+085	pg1307	13:09:47.01	+08:19:48.3	0.1550
PG1309+355	pg1309	13:12:17.80	+35:15:21.0	0.1550
SDSSJ135712.61+170444	s135712	13:57:12.61	+17:04:44.1	0.1500
PG1424+240	pg1424	14:27:00.39	+23:48:00.0	0.6035
MRK478	mrk478	14:42:07.47	+35:26:23.0	0.0791
TON236	ton236	15:28:40.60	+28:25:29.7	0.4500
1ES1553+113	1es1553	15:55:43.04	+11:11:24.4	0.4140
PG1626+554	pg1626	16:27:56.12	+55:22:31.5	0.1330
MRK1513	mrk1513	21:32:27.92	+10:08:18.7	0.0630
PG2349-014	pg2349	23:51:56.12	-01:09:13.1	0.1737

Note.
[a] Reference in Tables 4 and 5.

(This table is available in machine-readable form.)

between a galaxy's z_{phot} and its more secure z_{spec} in particular cases in the Appendix, but we do not use the z_{spec} values in our analysis. Given the completeness of the SDSS photometry, ~90% for galaxies to $r \sim 21.2$ (Rykoff et al. 2015), we estimate that the catalogs achieve the same completeness to $L \sim 0.3$–$0.5L^*$ for $z = 0.5$ and to $L \sim 0.01L^*$ for $z = 0.1$. The median redshift of the sample absorbers is 0.11.

3. Identifying Galaxy–Absorber Pairs

We use the linelists generated from the COS spectra of the QSO sightlines and provided as high-level science products through MAST and the SDSS photometry of the galaxies in those QSO fields as input into an algorithm that calculates a Bayesian probability that a particular absorption system is associated with each galaxy in the QSO field. The likelihoods draw upon previous work characterizing the distribution of absorber equivalent widths in various ionic species with galaxy impact parameter and intrinsic galaxy properties estimated from the SDSS photometry. Because we have only photometric redshifts for our sample galaxies, our objective is to define a statistic that will incorporate other available data such as absorber rest equivalent width, W, galaxy–absorber impact parameter, ρ, and galaxy properties such as virial radius r_{vir} or stellar mass M_* using empirical relationships derived from galaxy–absorber pairs identified by previous spectroscopic surveys.

The Bayesian statistic we define (Trotta 2017) is the posterior probability of a true match between an absorber and

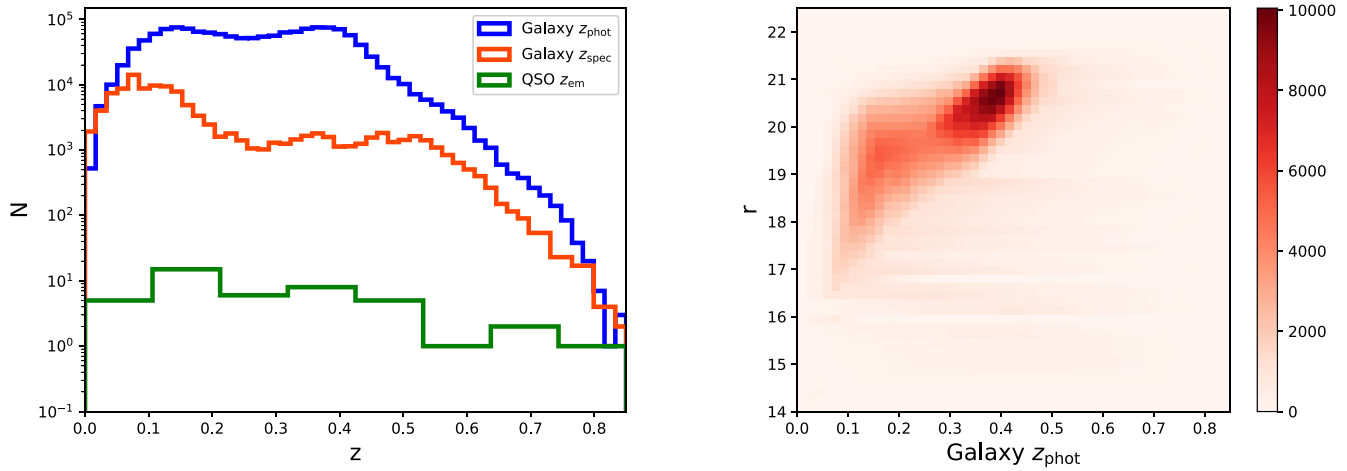

Figure 1. Left: Distribution of sample QSO emission redshifts (green); SDSS galaxy photometric redshifts (blue); and SDSS galaxy spectroscopic redshifts (red) Right: Distribution of sample SDSS galaxy r magnitudes and photometric redshifts.

galaxy i, given the combination of observed parameters: absorber W, galaxy–absorber ρ, and galaxy $r_{\rm vir}$ or M_*, expressed here as $\boldsymbol{p}$. The probability is multiplied over all ionic species, j:

$$P_i(m_z|p) = \frac{P_i(m_z)}{P(p)} \prod_j P_{ij}(p|m_z). \quad (1)$$

This statistic uses the prior $P_i(m_z)$ that galaxy i is a match for the absorber based on its photometric redshift alone, assuming Gaussian errors and integrated over $z_{\rm abs} \pm 500$ km s^{-1}.

The additional information about each potential galaxy–absorber pair, W, ρ, $r_{\rm vir}$, and M_* is contained in the likelihood, $P(p|m_z)$, the conditional probability of observing $\boldsymbol{p}$ given a galaxy–absorber relationship. This likelihood is calculated from a probability distribution that is assumed to be Gaussian, with parameters defined by the empirical relationships found for galaxy–absorber pairs in species j. Two definitions of $P(p|m_z)$ are described and investigated below. The posterior probability is normalized by summing over the possible outcomes, i.e., the absorber is matched to any one of the SDSS galaxies:

$$P(p) = \sum_i [P_i(m_z) \prod_j P_{ij}(p|m_z)]. \quad (2)$$

This construction makes the a priori assumption that each absorber in the QSO spectra can be attributed to the CGM of one of the SDSS galaxies in the field, i.e., it does not include a term accounting for the probability that the absorber is caused by the CGM of an undetected galaxy or is intergalactic in origin. However, in practice, the methodology described here does leave ∼40% of Lyα lines unpaired, indicating that they arise in the IGM or a galaxy fainter than the SDSS detection limit.

Our algorithms calculate the probability described in Equation (1) in a pairwise fashion. For each galaxy within a minimum impact parameter of the QSO sightline and judged on the basis of the photometric redshift to be in the QSO foreground, we calculate the probability of its association with each absorption system in the QSO spectrum, where absorption systems are defined here to be any group of features within 300 km s^{-1} of one another. The calculated galaxy–absorber impact parameter based on the photometric redshifts is necessarily uncertain, so we allow for this impact parameter to be as large as 2 Mpc. If the galaxy and absorber are truly "matched," they can be assumed to lie at approximately the same redshift, and so the impact parameter can be calculated instead from $z_{\rm abs}$. This $\rho(z_{\rm abs})$ is capped at 500 kpc. The addition of the empirical CGM ρ–W relationships provides further constraints on the statistical method.

The output of the algorithm is a list of up to 10 most probable galaxy matches to each absorption system. We preserve galaxy–absorber pairs with $P(m_z|p) > 0.1$. Because the probability defined in Equation (1) is a product over all ionic species in a system, the resulting value can be smaller than the probability calculated for individual ions. For these multicomponent systems, we preserve pairs for which the value of the probability for at least one Lyα component exceeds the 10% threshold. The algorithm often results in double matches, i.e., galaxies that are paired with more than one absorber in the top 10 list. To determine our final list of candidate galaxy–absorber pairs, we impose a uniqueness criterion that selects the highest-probability absorber paired with each galaxy, and that allows for lower-ranked galaxies to be associated with a particular absorption system if the galaxy with the highest probability is a better match for a different absorber. For this, we must compare different absorption system probabilities with one another, so again, we use the top Lyα component probability for multicomponent systems. This uniqueness criterion results in an absorber being paired with a galaxy that is first in its top 10 list about 61% of the time. In another ∼22 (9)% of cases, the galaxy selected as the unique match is the second (third) in the top 10 list.

We devised two different statistics based on Equation (1), each using a different construction of $P(p|m_z)$. One is based on the established empirical relationships between absorber equivalent width and galaxy–absorber impact parameter as a ratio with the galaxy's virial radius. We refer to this as the virial radius method. Our second statistic is based on the proposed CGM fundamental plane (Bordoloi et al. 2018), which also incorporates the galaxy stellar mass, and so this is labeled the stellar mass method.

3.1. Virial Radius Method

We use Equation (1) and linear fits to absorber rest equivalent width W versus galaxy–absorber impact parameter

Table 2
Galaxy–Absorber Pair Fits

Ion	W vs. $\rho/r_{\rm vir}$		W vs. ρ		ΔW vs. $\log M_*/M_\odot$	
	Slope	Intercept	Slope	Intercept	Slope	Intercept
H I	−0.553	−0.268	-1.02×10^{-2}	2.996	0.129	−1.492
O VI	−0.0114	−0.427	-1.68×10^{-2}	2.806	−0.199	1.702
C II	−0.663	−0.830	-4.75×10^{-2}	2.948	0.493	−0.348
C III	−0.523	−0.467	-1.30×10^{-2}	2.861	0.0459	−0.592
C IV	−0.358	−0.625	-3.28×10^{-2}	2.689	−0.121	1.0621
Si II	−0.718	−1.016	-4.85×10^{-2}	2.655	−0.0342	0.00864
Si III	−1.015	−1.048	-4.23×10^{-2}	2.841	0.0765	−1.170
Si IV	−1.016	−1.382	-4.50×10^{-2}	2.474	−0.169	1.517

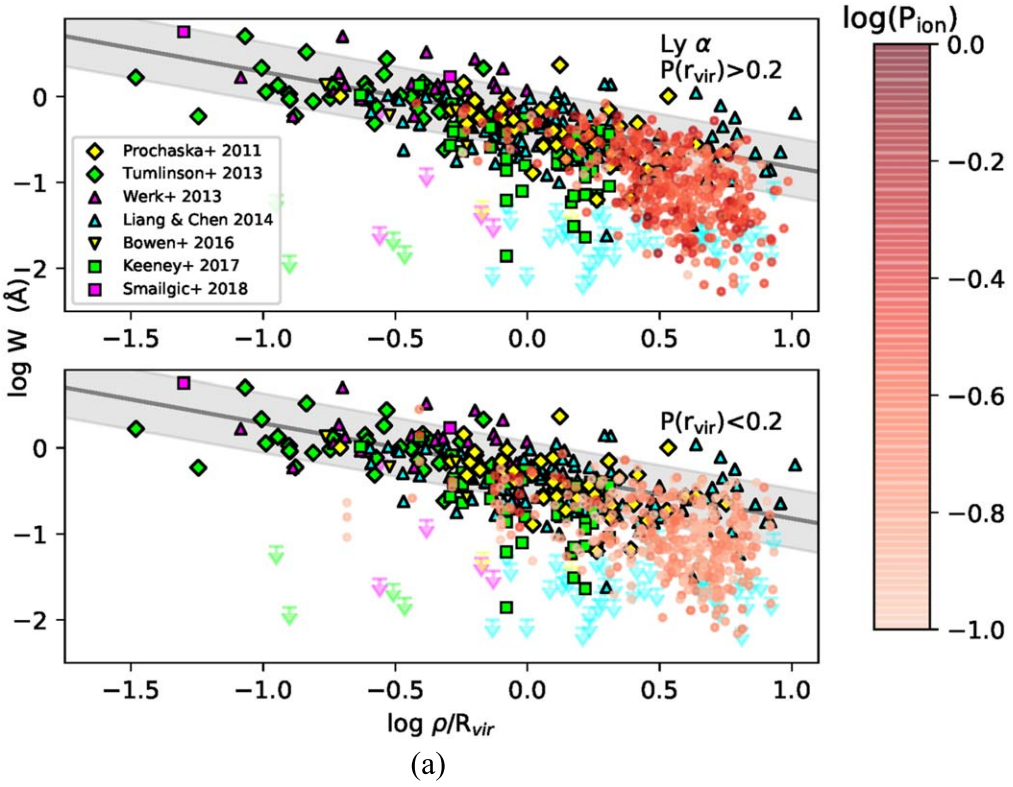

Figure 2. Absorber equivalent width vs. ratio of impact parameter to virial radius for all unique galaxy–absorber pairs for (a) Lyα (b) C II (c) Si II, (d) C III, (e) Si III, (f) C IV and (g) Si IV, and (h) O VI. Black lines and gray shaded regions show the fits to the literature points and 1σ confidence intervals. Red points are the unique galaxy–absorber pairs identified by the virial radius method, with shading indicating the value of $P_{\rm ion}$ ($=P(r_{\rm vir})$ for single-component Lyα absorbers). Other colors indicate upper limits from Prochaska et al. (2011b) (yellow), Werk et al. (2013) (magenta), Tumlinson et al. (2013) (green), and Liang & Chen (2014) (cyan). In panel (a), pairs with $P(r_{\rm vir}) > 0.2$ are shown on the top, and those with $P(r_{\rm vir}) < 0.2$ are on the bottom.

normalized by galaxy virial radius $\rho/r_{\rm vir}$ to define the statistic $P(r_{\rm vir})$. The parameters of the fits for each ion are listed in Table 2. We calculate $r_{\rm vir}$ using the Richter et al. (2016) parameterization of the Stocke et al. (2013) halo abundance matching curves.

Figure 2 shows the literature measurements for Lyα, O VI, C IV, C III, C II, Si IV, Si III, and Si II absorption paired with galaxies on the basis of spectroscopic redshifts. The fits to these points determine the parameters of the probability distribution for a given galaxy–absorber pair for each of the primary ionic species observed in the COS spectra. Fit parameters are listed in Table 2. The mean of the Gaussian probability density is the linear fit value for W given $\rho/r_{\rm vir}$ of the galaxy–absorber pair, and its variance is determined by the 1σ confidence region about the fit. In Figure 2, we also show upper equivalent width limits reported in the literature, but these points are not included in the fit. For Lyα, including these upper limits had no significant effect on the slope or the overall galaxy–absorber probability calculations. The metal line fits were more sensitive to these upper limits but resulted in a physically implausible positive slope for Si IV. The value of $P(p|m_z)$ is the integral, evaluated over $\pm 5\sigma_W$, of the product of this Gaussian probability density about the measured absorber equivalent width and a second Gaussian probability density associated with the measurement itself, i.e., with mean equal to $W_{\rm obs}$ and σ equal to the reported equivalent width error, σ_W.

The red points in Figure 2 mark the unique galaxy–absorber candidate pairs identified by the virial radius method, with shading indicating the value of the probability used in the uniqueness criterion, $P_{\rm ion}$. This is the same as the overall

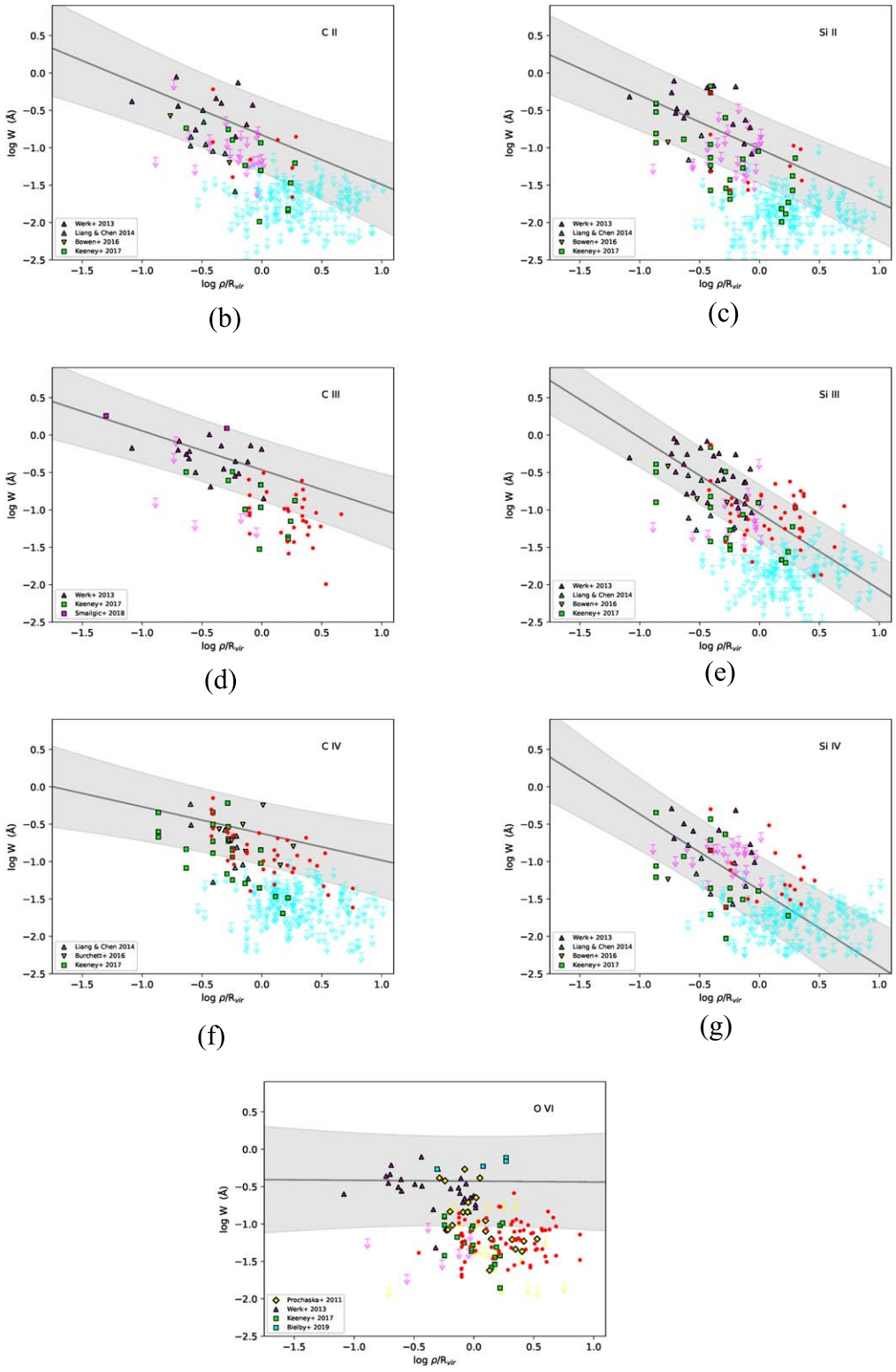

Figure 2. (Continued.)

probability, $P(r_{\rm vir})$, for absorbers consisting of a single Lyα line, but is the value of the largest Lyα component probability for multicomponent systems. For Lyα, the pairs shown in the top panel correspond to those with overall probability $P(r_{\rm vir}) > 0.1$. Pairs marked by shaded red points in the bottom panel have $P(r_{\rm vir}) < 0.1$. Due to the imposition of the 10% threshold to select only the most reasonable candidate pairs, the points in this bottom panel correspond to multicomponent absorption systems. In other words, no galaxies paired with single Lyα absorbers with $P(r_{\rm vir}) < 0.1$ are part of our final candidate lists.

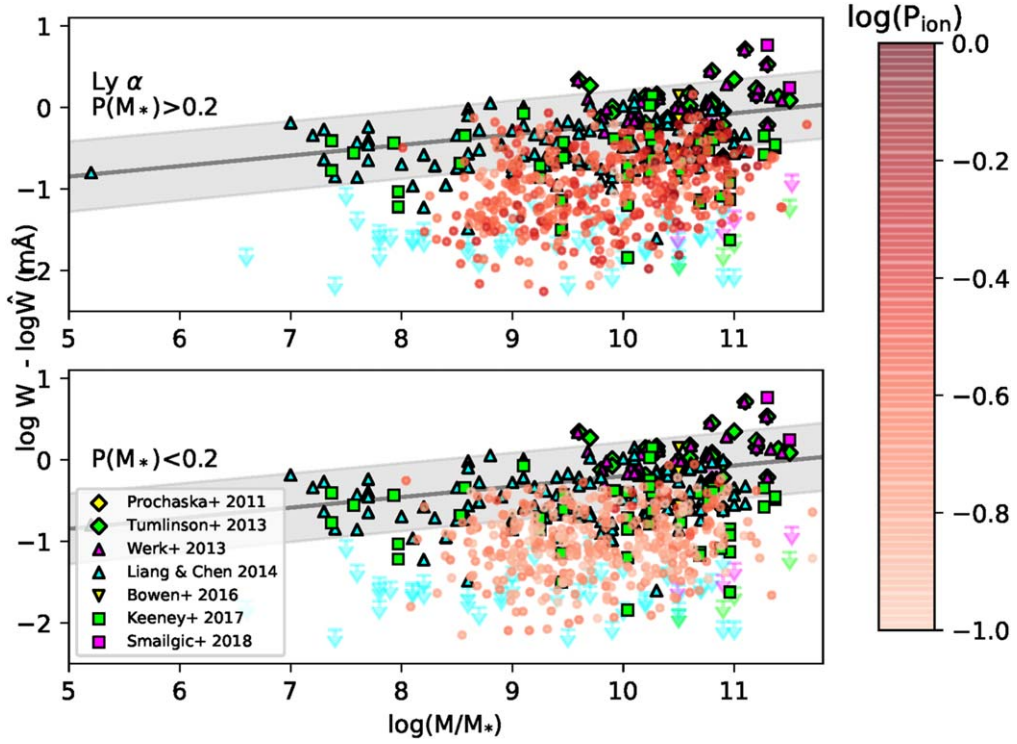

(a)

Figure 3. Difference of absorber equivalent width and $\hat{W}$ vs. galaxy stellar mass in solar masses for all unique galaxy–absorber pairs for (a) Lyα (b) C II (c) Si II, (d) C III, (e) Si III, (f) C IV, (g) Si IV, and (h) O VI. Black lines and gray shaded regions show the fits to the literature points and 1σ confidence intervals. Red points are the unique galaxy–absorber pairs identified by the virial radius method, with shading indicating the value of $P_{\rm ion}$ (=$P(M_*)$ for single-component Lyα absorbers). Other colors indicate upper limits from Prochaska et al. (2011b) (yellow), Werk et al. (2013) (magenta), Tumlinson et al. (2013) (green), and Liang & Chen (2014) (cyan). In panel (a), pairs with $P(M_*) > 0.2$ are shown on the top, and those with $P(M_*) < 0.2$ are on the bottom.

3.2. Stellar Mass Method

The second statistic we define, $P(M_*)$, uses the CGM fundamental plane, a relationship between absorber equivalent width, galaxy–absorber impact parameter, and galaxy stellar mass proposed by Bordoloi et al. (2018). Similar to the virial radius method, the $P(p|m_z)$ term in Equation (1) is calculated from a Gaussian probability function with mean determined from a linear fit to $\log W - \log \hat{W}$ versus $\log M_*/M_\odot$, where $\hat{W}$ is itself found from a linear fit to W versus impact parameter ρ, and galaxy stellar masses are estimated from the SDSS photometry using the prescription of Taylor et al. (2011). The 1σ confidence limit on the linear fit sets the width of the probability distribution, and the value of $P(p|m_z)$ is calculated from the integral about the observed absorber equivalent width. Bordoloi et al. (2018) developed the fundamental plane for the ubiquitous Lyα CGM absorption and its clear dependence on galaxy stellar mass. We extend that formalism to all the ions considered. Fit parameters are listed in Table 2, and the results are shown in Figure 3, with top and bottom sections for $P(M_*) > 0.2$ and $P(M_*) > 0.2$ as defined in Figure 2(a).

4. Results

Using each of the two methods described above, we identify the 10 most probable galaxy matches to each absorber or absorption system, for all $P(r_{\rm vir}) > 0$ or $P(M_*) > 0$. Both methods method resulted in 1026 absorbers in the COS sample, including 136 metal line systems, matched to at least one SDSS galaxy. From among these top 10 matches, we identify unique candidate galaxy–absorber pairs. Table 3 lists the characteristics of the galaxies, absorbers, and pairs in the virial radius method candidate list. Values are the same for the pairs found using the stellar mass method, unless otherwise noted.

As discussed above, the product of $P_{\rm ion}$, or P_j as expressed in Equation (1), over all ionic species results in a smaller value for the overall probability, $P(r_{\rm vir})$ or $P(M_*)$, for multicomponent absorption systems. This is consistent with the additional constraints provided by the combination of several ions. However, this does mean that only relative comparisons of the total probability, $P(r_{\rm vir})$ or $P(M_*)$, for different galaxy matches to the same absorber, are possible. In our assignment of unique individual galaxy–absorber pairs, we must assess the relative strength of different galaxy–absorber matches, and so for this we use the value of $P(r_{\rm vir})$ or $P(M_*)$ of Lyα only in the case of a multicomponent system, so that the presence of metals does not penalize a particular absorber in the ranking, when in fact the presence of metals should improve the chances that it is associated with a galaxy.

The 849 Lyα lines in 636 unique galaxy–absorber pairs satisfying the 10% probability criterion identified with virial radius method are shown as red points, in Figure 2 and tabulated in Table 4. In Figure 2(a), we show the results for Lyα, shaded by the value of $P(r_{\rm vir})$. Of these candidate pairs, 87 of the absorbers are metal line systems. Table 5 lists the 632 galaxy–absorber pairs comprising 831 Lyα lines identified using the CGM fundamental plane, the stellar mass method. These pairs are shown in Figure 3. Of these candidate pairs, 83 of the absorbers are metal line systems. The red points in Figures 2 and 3 do generally lie within the confidence limits on the fits to the literature pairs listed in Table 2, but linear fits to

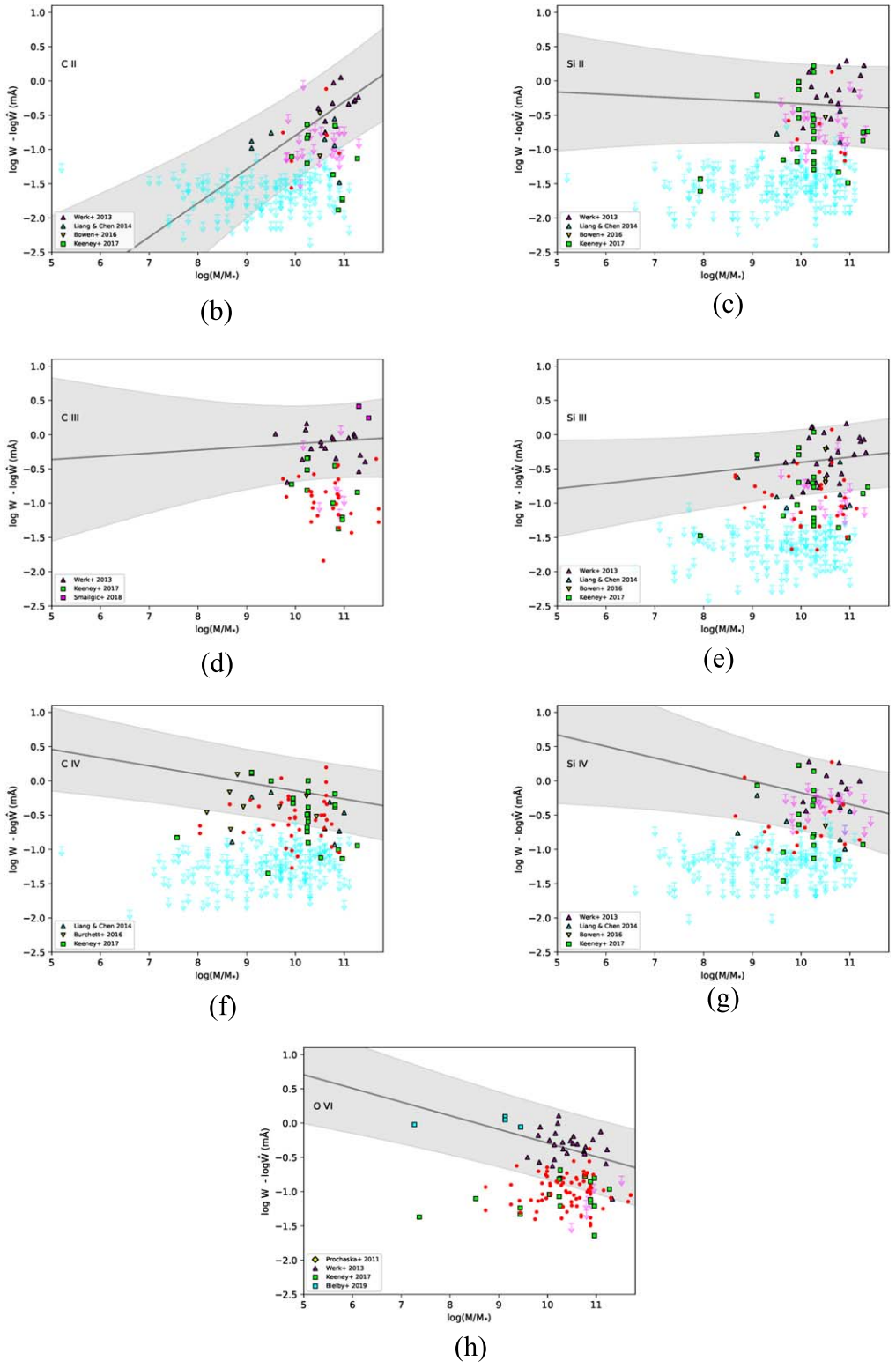

Figure 3. (Continued.)

the results for each ion do yield different slopes and intercepts. However, there is no systematic difference, and this is likely due to the relative lack of results at low impact parameters.

The galaxies for which there is a spectroscopic redshift measured by SDSS provide a useful check on our methods. For those 222 galaxies, in pairs identified by the two methods, the galaxy spectroscopic redshift lies within 400 km s^{-1} of the absorber redshift in 55 (57) of the cases for the virial radius (stellar mass) method, indicating that our candidate galaxy–absorber pair lists may contain a fairly high rate of spurious matches. The rate of velocity misalignment is ∼48%–57% if we consider only pairs with $\rho < 200$ kpc or $\rho/r_{\rm vir} < 2$ or absorbers with $W > 200$ mÅ, which constitute 10%, 12%, and 23%, respectively, of the pairs in Table 4, and 11%, 14%, and

Table 3
Distributions of Galaxy–Absorber Pair Characteristics[a]

	Min.	Med.	Max.
Galaxies			
M_r	−23.0	−19.9(−20.0)	−15.9
$u-r$	0.57	1.7	6.9
$\log M_*/M_\odot$	8.0	9.7	11.7
Absorbers			
z_{abs}	0.0016	0.11	0.47[b]
W(Lyα) (m Å)	5.3	92	2800(1400)
Pairs			
ρ (kpc)	29(19)	430	500[c]

Notes.
[a] Values are the same for the pairs found by both methods, otherwise listed separately for pairs found by the virial radius(stellar mass) method.
[b] $z = 0.5$ is imposed as the maximum redshift for galaxy–absorber pairs.
[c] A maximum impact parameter $\rho = 500$ kpc is imposed by both the virial radius and stellar mass algorithms.

23% of those listed in Table 5. For metal line systems, the overall rates of velocity misalignments are 35% and 29%, respectively, for the two methods. The SDSS spectroscopic redshift measurements are primarily concentrated in the lower-redshift half of our sample $z < 0.1$, where the offsets with photometric redshifts are large compared to the photometric redshift error (Beck et al. 2016). Thus, the false-positive rate may be lower than estimated here in the overall candidate list.

Individual sightlines are discussed in the Appendix. These notes highlight the importance of investigating both the ranked galaxy–absorber outcomes of the methods and the final galaxy–absorber pairs after the uniqueness criterion has been imposed. Galaxies particularly worthy of follow-up investigations are noted.

4.1. Comparison with the Literature

Our virial radius and stellar mass Bayesian methods identified 402 and 411 candidate galaxy–absorber pairs, respectively, along the QSO lines of sight in common with previous studies. Specific comparisons with 81 pairs found by previous studies are tabulated in Table 6. In 34 cases, the galaxy is excluded from our catalog of SDSS galaxies, usually on the basis of the photometric redshift quality cut we employed. Of the 47 pairs for which the galaxy is part of our SDSS catalog, we recover the galaxy–absorber pair as the top ranked match with one or both methods in 19 cases, and in another 15 cases, the pair was recovered but with a lower ranking for both methods. The 13 unrecovered pairs are due to either an impact parameter larger than our threshold of 500 kpc or to a large mismatch between the photometric and spectroscopic redshifts, which by construction has been measured for all of these galaxies. Our methods do not use the spectroscopic redshifts even when available, but they do provide insight into why we do not recover all the pairings found in the targeted studies. The cases in which the poor photometric redshift estimate is the reason we do not recover a pair correspond to galaxies with $z < 0.01$ where the photometric redshift techniques are expected to have trouble given their overall accuracy. Nevertheless, there are several cases listed in Table 6 of $z < 0.01$ galaxy–absorber pairs that are recovered by our method, even as the top-ranked match. These QSO fields are discussed in detail in the Appendix, along with all the others in our sample.

In a large study of galaxy redshifts in QSO fields, Keeney et al. (2018) report spectroscopic redshifts for galaxies in 25 of our fields and flag the galaxies that are closest to an absorber in their Table 6. For the galaxy–absorber pairs in our Tables 4 and 5 that are in common with their sample, we reproduce their flag in Column 17 and we discuss the cases in which these new spectroscopic measurements confirm or refute our candidate galaxy–absorber pairs. The comparison with the Keeney et al. (2018) results is a useful exercise for both demonstrating the reliability of these methods and uncovering cases in which our methods would recommend spectroscopic follow-up that was not included in their sample. Our methods recover 86% of the galaxies in their Table 6 that have an impact parameter less than 500 kpc and are flagged as the closest galaxy to an absorber (their flag 3) to be a member of a candidate galaxy–absorber pair. Including galaxies within 500 kpc that these authors mark as lying within 1000 km s^{-1} of an absorber but not necessarily the closest galaxy to an absorber, their flags 1 or 2, we recover 73%.

4.2. Galaxy Properties

In Figure 4, we show the distributions in galaxy–absorber impact parameter and Lyα rest equivalent width for the unique galaxy–absorber pairs identified by both methods. To investigate trends with galaxy properties, the sample is divided into red and blue, i.e., $u-r$ greater or less than 2.2, to approximately delineate early and late morphological types (Strateva et al. 2001). We also compare low- and high-luminosity galaxies, defined here as less or greater than $0.1L^*$. There is a distinct difference in the equivalent width distributions for these two subsamples, in the sense that redder and more luminous galaxies show larger equivalent width absorption at lower impact parameter. The median values of ρ/r_{vir} differ by a factor $\sim$1.5 for the red versus blue (2.9 versus 4.5) and by a factor of $\sim$1.7 for higher- versus lower-luminosity (3.1 versus 5.4) subsamples. Table 7 lists the results of Kolmogorov–Smirnov tests, indicating that these samples are not drawn from the same parent distribution. The most plausible CGM absorbers arising from our analysis are those pairs with impact parameter within $2r_{vir}$, which are approximately evenly split between the red and blue subsamples, but dominated by $> 0.1L^*$ galaxies.

To test the robustness of these conclusions, we generated 100 realizations of random pairings between the Lyα absorbers in our final samples of unique pairs and SDSS galaxies that lie within 500 kpc of the QSOs. The impact parameter distributions for red versus blue and high- versus low-luminosity subsamples as defined above are shifted to smaller impact parameter and less distinctly bimodal than the distributions of hits versus misses, with medians of 2.0 kpc (2.4 kpc) for red (blue) and 3.1 kpc (2.0 kpc) for high (low) luminosity.

In Figure 5, we compare the properties of galaxies within 500 kpc of the QSOs that are found to be paired with Lyα absorbers using both methods, versus those that are not paired with any absorber. We label the former "hits" and the latter "misses," somewhat similarly to Stocke et al. (2013), who define a "miss" to be a super-L^* galaxy with $\rho \leqslant 1$ Mpc that shows no absorption in the QSO spectrum. However, we

Table 4
Galaxy–Absorber Pairs: P(r_{vir})

QSO	P_{tot}	ρ (kpc)	Ion	z_{abs}	W (mÅ)	σ_W (mÅ)	P_{ion}	z_{phot}	R.A. (deg)	Decl. (deg)	r	M_r	r_{vir} (kpc)	$\log M_*/M_\odot$	SDSS ID	K18 Flag[a]
1es1028	2.5207E-01	254.687	Lyα	2.427E-03	89.782	12.969	2.671E-01	2.154E-02	158.921	50.100	16.465	−18.431	70.329	9.032	1237657630058938491	⋯
1es1028	2.5207E-01	254.687	Lyα	3.224E-03	270.129	28.907	8.360E-02	2.154E-02	158.921	50.100	16.465	−18.431	70.329	9.032	1237657630058938491	⋯
1es1028	1.1958E-01	343.842	Lyα	2.188E-02	79.266	8.807	1.731E-01	2.114E-02	157.506	50.847	15.275	−19.579	91.705	9.536	1237658800956833843	⋯
1es1028	1.1958E-01	343.842	Lyα	2.258E-02	86.057	9.779	1.785E-01	2.114E-02	157.506	50.847	15.275	−19.579	91.705	9.536	1237658800956833843	⋯
1es1028	1.0094E-01	371.030	Lyα	4.484E-02	135.906	21.056	1.009E-01	1.033E-01	157.917	50.995	19.433	−18.974	79.386	9.090	1237658800956965095	1
1es1028	6.0033E-01	447.070	Lyα	5.098E-02	194.105	9.515	6.003E-01	4.761E-02	157.988	50.965	17.823	−18.847	77.109	9.053	1237658800956965110	2
1es1028	1.8408E-01	335.835	Lyα	7.604E-02	35.315	13.011	1.841E-01	1.739E-01	157.729	50.911	19.989	−19.632	92.899	9.806	1237658800956899418	⋯
1es1028	1.1389E-01	477.845	Lyα	8.836E-02	78.099	12.863	1.139E-01	1.649E-01	157.905	50.831	18.799	−20.787	125.474	10.287	1237657589242331520	3
1es1028	1.2180E-01	479.116	Lyα	1.071E-01	86.713	7.226	1.218E-01	1.739E-01	157.779	50.954	19.406	−20.316	110.620	10.152	1237658800956899891	⋯
1es1028	2.1460E-01	469.197	Lyα	1.125E-01	115.956	12.584	2.146E-01	1.552E-01	157.732	50.913	19.508	−19.804	96.968	9.525	1237658800956899417	3

Note.
[a] Absorption flag as in Keeney et al. (2018): –1 = object has $z < 0.001$ and is likely a star; 0 = galaxy is not within 1000 km s^{-1} of an absorber; 1 = galaxy is within 1000 km s^{-1} of an absorber but is not the closest galaxy; 2 = galaxy is closest in this table to an absorber, but a closer galaxy is known from SDSS or other sources; 3 = closest known galaxy to an absorber.

(This table is available in its entirety in machine-readable form.)

Table 5
Galaxy–Absorber Pairs: P(M_*)

QSO	P_{tot}	ρ (kpc)	Ion	z_{abs}	W (mÅ)	σ_W (mÅ)	P_{ion}	z_{phot}	R.A. (deg)	Decl. (deg)	r	M_r	r_{vir} (kpc)	$\log M_*/M_\odot$	SDSS ID	K18 Flag[a]
1es1028	1.4423E-01	50.251	Lyα	2.427E-03	89.782	12.969	1.322E-01	2.114E-02	157.506	50.847	15.275	−19.579	91.705	9.536	1237658800956833843	⋯
1es1028	1.4423E-01	50.251	Lyα	3.224E-03	270.129	28.907	2.023E-01	2.114E-02	157.506	50.847	15.275	−19.579	91.705	9.536	1237658800956833843	⋯
1es1028	1.7174E-01	434.062	Lyα	2.188E-02	79.266	8.807	1.803E-01	3.214E-02	157.440	50.797	15.772	−20.018	102.384	9.779	1237658800956833808	⋯
1es1028	1.7174E-01	434.062	Lyα	2.258E-02	86.057	9.779	1.830E-01	3.214E-02	157.440	50.797	15.772	−20.018	102.384	9.779	1237658800956833808	⋯
1es1028	6.0011E-01	447.070	Lyα	5.098E-02	194.105	9.515	6.001E-01	4.761E-02	157.988	50.965	17.823	−18.847	77.109	9.053	1237658800956965110	2
1es1028	1.1362E-01	444.346	Lyα	7.604E-02	35.315	13.011	1.136E-01	2.860E-01	157.903	50.964	20.549	−20.139	105.635	9.487	1237658800956965086	⋯
1es1028	1.1236E-01	477.845	Lyα	8.836E-02	78.099	12.863	1.124E-01	1.649E-01	157.905	50.831	18.799	−20.787	125.474	10.287	1237657589242331520	3
1es1028	1.6630E-01	408.069	Lyα	9.436E-02	101.429	9.138	1.663E-01	1.739E-01	157.729	50.911	19.989	−19.632	92.899	9.806	1237658800956899418	⋯
1es1028	1.1417E-01	479.116	Lyα	1.071E-01	86.713	7.226	1.142E-01	1.739E-01	157.779	50.954	19.406	−20.316	110.620	10.152	1237658800956899891	⋯
1es1028	2.0735E-01	469.197	Lyα	1.125E-01	115.956	12.584	2.074E-01	1.552E-01	157.732	50.913	19.508	−19.804	96.968	9.525	1237658800956899417	3

Note.
[a] Absorption flag as in Keeney et al. (2018): –1 = object has $z < 0.001$ and is likely a star; 0 = galaxy is not within 1000 km s^{-1} of an absorber; 1 = galaxy is within 1000 km s^{-1} of an absorber but is not the closest galaxy; 2 = galaxy is closest in this table to an absorber, but a closer galaxy is known from SDSS or other sources; 3 = closest known galaxy to an absorber.

(This table is available in its entirety in machine-readable form.)

Table 6
Galaxy–Absorber Pairs in the Literature

QSO	ρ (kpc)	Galaxy	Mag. Filter	z_{gal}	z_{abs}	W[a] (mÅ)	σ_W[a] (mÅ)	Ref.[b]	SDSS Note[c]	Rank[d] (r_{vir})	Rank[d] (M_*)	z_{phot}
1ES 1028+511	90	UGC 5740	15.1B	0.00216	0.00243	13.5	0.19	S13	3			
1ES 1028+511	25	SDSS J103108.88+504708.7	16.3g	0.00311	0.00320	17.2	22	S13	3			
1ES 1028+511	279	SDSS J103110.35+505211.0	18.4g	0.137	0.137	238	10	LC14	1	1	1	0.136
1SAX J1032.3+5051	65	UGC 5740	15.1B	0.00216	0.00239	13.1	3.5	S13	3			
3C 273	69	SDSS J122815.96+014944.1	16.5g	0.00303	0.00340	393	8	LC14	1	1	1	0.0136
3C 273	118	SDSS J123103.89+014034.4	14.8B	0.00368	0.00337	350	36	B96,P02,S13	3			
3C 273	126	SDSS J122745.86+013601.8	17.0B	0.00431	0.00528	410	⋯	B96,P02	3			
3C 273	288	NGC 4420	12.7g	0.00565	0.00529	15.38	0.34	S13	2			
3C 273	80	SDSS J122950.57+020153.7	17.3g	0.00592	0.00529	15.38	0.34	S13	1	⋯	⋯	0.0362
3C 273	771	UGC 7625	16.7g	0.00745	0.00720	20	5	P02,WS09	3			
3C 273	429	SDSS J122815.88+024202.9	15.4g	0.00762	0.00758	31	7	WS09	1	1	1	0.019
FBQS J1010+3003	48	UGC 5478	14.3B	0.00459	0.00462	17.8	3.5	S13	3			
FBQS J1010+3003	181	SDSS J101008.85+300252.5	18.6g	0.0874	0.0875	329	12	LC14	1	7	7	0.111
FBQS J1010+3003	252	SDSS J100953.51+300202.2	17.5g	0.113	0.114	254	15	LC14	1	⋯	6	0.0957
MRK 106	1030	UGC 4800	14.6B	0.00811	0.00803	77[e]	12	WS09	3			
MRK 106	418	SDSS J091923.29+553137.2	16.6g	0.0318	0.0317	217	6	LC14	3			
MRK 478	645	NGC 5727	14.2B	0.00497	0.00525	254	14	WS09	1	⋯	⋯	0.198
PG 0003+158	193	SDSS J000556.15+160804.1	17.4g	0.0909	0.0909	805	8	LC14	1	6	1	0.087
PG 0026+129	111	WISEA J002915.37+132056.5	15.8B	0.0394	0.0391	444	16	B97,D16	1	2	2	0.028
PG 0832+251	263	SDSS J083335.65+250847.1	18.1g	0.00743	0.00730	248	11	LC14	3			
PG 0832+251	53	NGC 2611	14.9g	0.0174	0.0174	18.4	0.2	S13	1	2	1	0.027
PG 0832+251	283	SDSS J083607.41+250645.7	15.5g	0.0232	0.0233	160	13	LC14	1	2	2	0.0230
PG 0844+349	250	NGC 2683	10.2B	0.00137	0.00137	25[e]	8	WS09	2			
PG 0844+349	372	UGC 4621	13.9B	0.00769	0.00754	6[e]	5	WS09	2			
PG 0953+414	296	NGC 3104	13.6B	0.00204	0.00204	70	9	WS09	2			
PG 0953+414	435	SDSS J095638.90+411646.0	17.6g	0.143	0.142	268	5	S13,LC14	1	7	3	0.132
PG 1001+291	84	UGC 5427	14.6B	0.00165	0.00165	308	112	WS09	3			
PG 1001+291	337	UGC 5464	15.8g	0.00337	0.00357	267	14	WS09	1	7	7	0.0236
PG 1001+291	167	SDSS J100618.16+285641.9	14.4g	0.00454	0.0036	297	23	B97,LC14	3			
PG 1001+291	1249	UGC 5461	15.5g	0.0160	0.0153	242	11	WS09	1	⋯	⋯	0.0350
PG 1001+291	179	SDSS J100403.24+285650.2	18.6g	0.133	0.134	177	9	LC14	1	1	1	0.143
PG 1001+291	57	SDSS J100402.36+285512.5	22.3g	0.138	0.137	776	18	M14	3			
PG 1001+291	222	TON0028:[KSS94] 39	22.4g	0.214	0.214	736	55	M14	4			
PG 1048+342	465	SDSS J105111.41+335935.6	15.8g	0.0596	0.0593	270	8	LC14	1	1	2	0.0601
PG 1116+215	543	UGC 6258	14.9B	0.00485	0.00493	91	10	WS09	1	⋯	⋯	0.0140
PG 1116+215	1742	NGC 3649	14.6B	0.0166	0.0163	111	12	WS09	3			
PG 1116+215	557	SDSS J112045.94+211115.3	18.1g	0.0210	0.0195	167	24	T98	1	⋯	⋯	0.0217
PG 1116+215	388	SDSS J111843.28+212723.0	17.1B	0.0323	0.0322	108	6	LC14	1	1	1	0.0343
PG 1116+215	746	SDSS J111909.56+210243.4	18.1g	0.0410	0.0412	164	37	T98	1	⋯	⋯	0.0505
PG 1116+215	601	SDSS J111924.26+211029.9	16.6g	0.0590	0.0590	157	24	T98	1	⋯	⋯	0.0687
PG 1116+215	256	SDSS J111905.34+211537.7	17.2B	0.0590	0.0590	13.5	0.1	S13	1	7	6	0.0411
PG 1116+215	131	SDSS J111905.51+211733.0	19.3g	0.0600	0.0590	13.5	0.1	S13	1	⋯	10	0.0983
PG 1116+215	677	SDSS J111942.04+212610.3	19.3g	0.0613	0.0608	62	22	T98	1	⋯	⋯	0.0904
PG 1116+215	138	SDSS J111906.68+211828.7	18.1B	0.138	0.138	471	5	LC14	1	4	1	0.134
PG 1121+422	123	SDSS J112418.74+420323.1	17.8g	0.0245	0.0245	512	9	LC14	1	1	1	0.0325
PG 1121+422	213	SDSS J112457.15+420550.8	17.1g	0.0337	0.0338	198	6	LC14	1	2	2	0.0421
PG 1216+069	12	VCC 381	16.6HI	0.00160	0.00550	1630	160	B96	3			

Table 6
(Continued)

QSO	ρ (kpc)	Galaxy	Mag. Filter	z_{gal}	z_{abs}	W[a] (mÅ)	σ_W[a] (mÅ)	Ref.[b]	SDSS Note[c]	Rank[d] (r_{vir})	Rank[d] (M_*)	z_{phot}
PG 1216+069	77	VCC 538	15.4B	0.00167	0.00550	1630	160	B96	1	⋯	⋯	0.384
PG 1216+069	42	IC 3115	13.7B	0.00244	0.00550	1630	160	B96	2			
PG 1216+069	72	VCC 446	15.5B	0.00283	0.00550	1630	160	B96	1	9	⋯	0.0128
PG 1216+069	146	UGC 7423	15.6B	0.00419	0.00550	1630	160	B96	1	⋯	⋯	0.0243
PG 1216+069	192	VCC 340	15.4B	0.00504	0.00550	1630	160	B96	1	10	⋯	0.0116
PG 1216+069	184	VCC 329	16.8B	0.00541	0.00550	1630	160	B96	1	⋯	⋯	0.0913
PG 1216+069	184	NGC 4260	12.7B	0.00653	0.00550	1630	160	B96	2			
PG 1216+069	207	VCC 223	16.5B	0.00690	0.00550	1630	160	B96	1	⋯	⋯	0.0159
PG 1216+069	185	NGC 4241	13.0B	0.00745	0.00550	1630	160	B96	2			
PG 1216+069	16	VCC 415	15.1B	0.00854	0.00550	1630	160	B96	3			
PG 1216+069	344	SDSS J121930.87+064334.4	16.3g	0.0799	0.0794	520	110	B96	3			
PG 1216+069	344	SDSS J121930.87+064334.4	16.3g	0.0799	0.0784	450	110	B96	3			
PG 1216+069	500	SDSS J121930.86+064334.4	16.2g	0.0804	0.0805	13.87	0.28	S13	3			
PG 1216+069	95	SDSS J121923.43+063819.7	18.0R	0.1242	0.124	1376	173	M14	1	6	1	0.132
PG 1229+204	112	UGC 7697	15.0B	0.00846	0.00859	290	70	C05	3			
PG 1259+593	58	SDSS J130207.44+584153.8	14.4g	0.00221	0.00229	13.83	0.24	S13	3			
PG 1259+593	55	UGC 8146	14.4B	0.00223	0.00226	330	80	C05	3			
PG 1259+593	595	UGC 8040	14.7B	0.00841	0.00759	291	11	WS09	1	5	5	0.0194
PG 1259+593	136	SDSS J130101.05+590007.1	17.1g	0.0462	0.0460	15.51	0.28	S13	1	1	1	0.0433
PG 1259+593	135	SDSS J130116.43+590135.7	21.6g	0.197	0.196	44	24	M14	1	7	8	0.352
PG 1259+593	280	SDSS J130109.88+590315.3	20.6g	0.241	0.241	49	15	M14	1	5	5	0.292
PG 2349-014	198	SDSS J235142.21-010100.9	17.1g	0.0385	0.0381	418	41	B97,D16	1	1	1	0.0433
Q 1230+115	339	UGC 7625	16.7g	0.00745	0.00769	338	21	P02,WS09	1	⋯	⋯	0.114
SBS 1108+560	20	M 108	10.7B	0.00232	0.00222	14.3	4.0	S13	2			
SBS 1108+560	20	M 108	10.7B	0.00232	0.00259	14.2	4.0	S13	2			
SBS 1108+560	437	WISEA J111125.60+554435.4	18.4g	0.137	0.138	542	5	LC14	1	1	1	0.133
SBS 1122+594	32	IC 691	14.2g	0.00401	0.004	993	15	S13,LC14	2			
SBS 1122+594	336	SDSS J112517.67+590828.8	17.2g	0.0578	0.0578	236	11	LC14	1	1	1	0.0645
SDSS J080908.13+461925.6	63	SDSS J080913.17+461842.7	17.1g	0.0466	0.0464	1026	10	LC14	1	1	2	0.0636
SDSS J092554.43+453544	342	SDSS J092721.06+454158.8	17.1g	0.0171	0.0170	183	10	LC14	1	2	2	0.0338
SDSS J092554.43+453544	244	SDSS J092617.38+452924.9	17.1g	0.0270	0.0261	453	10	LC14	1	1	2	0.0326
SDSS J094952.91+390203	166	SDSS J095002.76+390308.7	17.8g	0.0658	0.0669	165	12	LC14	1	1	1	0.0584
TON 236	193	SDSS J152827.39+282738.6	18.4g	0.0451	0.0451	160	8	LC14	3			
TON 580	249	SDSS J113056.11+311445.6	18.5g	0.0745	0.0744	324	11	LC14	1	1	1	0.0872

Notes.

[a] Lyman α rest equivalent width. For Stocke et al. (2013) entries, these columns list $\log N_{H\,I}$ and its error.

[b] B97: Bowen et al. (1997); T98: Tripp et al. (1998); P02 Penton et al. (2002); C05 Côté et al. (2005); WS09: Wakker & Savage (2009); S13: Stocke et al. (2013); LC14: Liang & Chen (2014); M14: Mathes et al. (2014); D16: Danforth et al. (2016).

[c] Galaxy is present in SDSS catalog (1); galaxy is not in SDSS catalog, $r < 14$ (2); photometric redshift cut (3); no photometric redshift (4).

[d] Rank of galaxy–absorber pair with $P(r_{vir})$ or $P(M_*)$. No entry indicates that this galaxy is not recovered in the top 10 highest probability matches to the absorber for that method.

[e] Lyman β.

(This table is available in machine-readable form.)

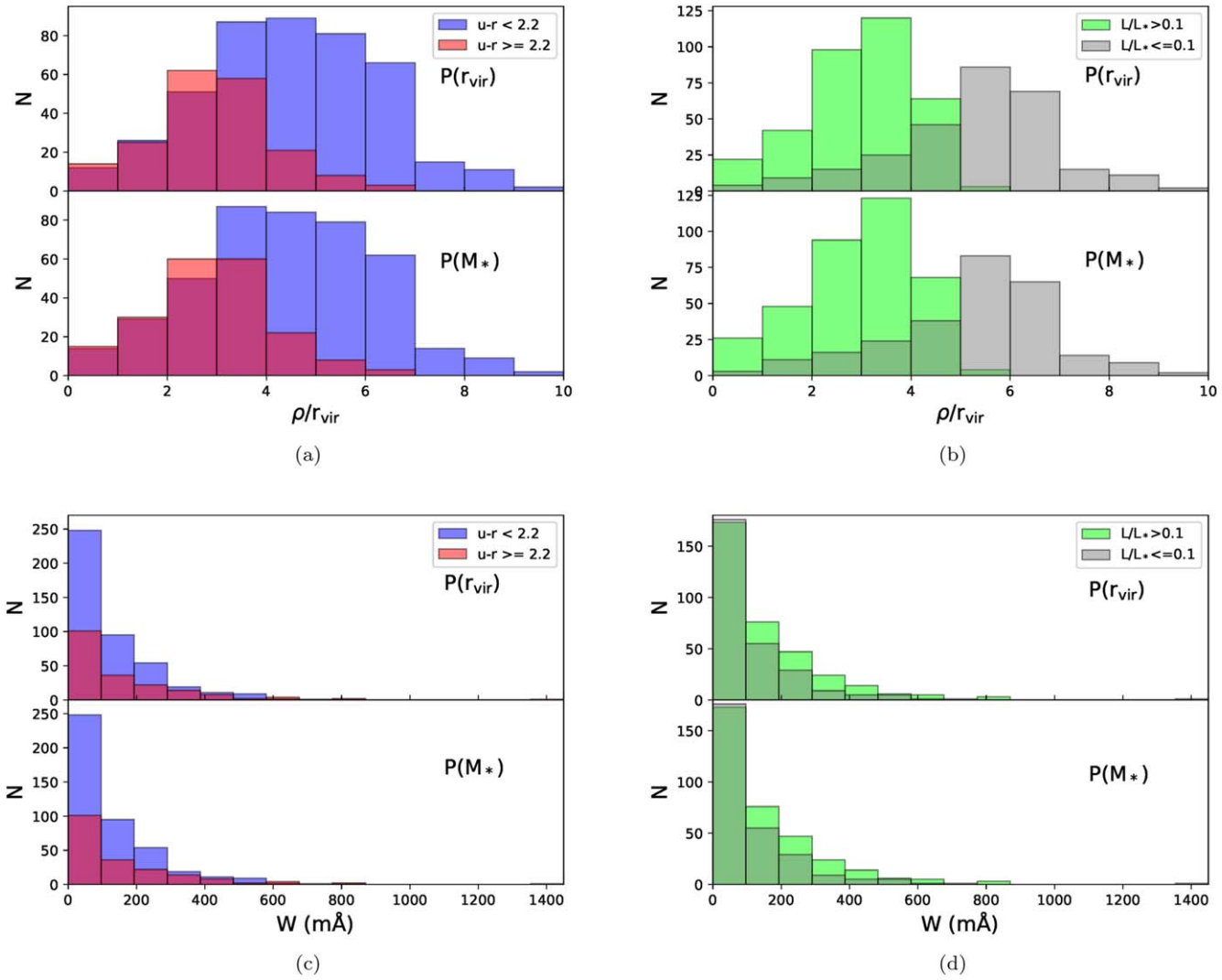

Figure 4. Distributions of galaxy–absorber impact parameter for (a) red ($u-r>2.2$) vs. blue galaxies and for (b) low- ($L/L^{*}<0.1$) vs. high-luminosity galaxies. Distributions of absorber rest Lyα equivalent width for (c) red ($u-r>2.2$) vs. blue galaxies and for (d) low- ($L/L^{*}<0.1$) vs. high-luminosity galaxies.

consider the entire SDSS photometric sample, and our galaxy–absorber associations, or lack thereof, are less secure than in spectroscopic surveys of galaxies in QSO fields. The galaxy properties we explore here include those discussed previously, impact parameter normalized by galaxy virial radius, $u-r$ as a proxy for morphological type, and the stellar mass estimated from the $g-i$ color (Taylor et al. 2011). We also include here an estimate of the galaxy orientation to the QSO, ϕ, defined to be between 0° for a galaxy with its major axis aligned with the galaxy–QSO direction and 90° for one with its minor axis aligned as such. There is evidence of a difference in the distributions in $\rho/r_{\rm vir}$, $u-r$, and stellar mass, in the sense that the hits are bluer (median $u-r=1.8$ versus 2.3), lower in stellar mass (median $\log(M_{*}/M_{\odot})=9.8$ versus 10.2) and found at larger impact parameter than misses (median $\rho/r_{\rm vir}=1.9$ versus 1.5). For metal line systems, however, there is a preference for smaller impact parameter among the hits, median $\rho/r_{\rm vir}=1.2$ versus 1.8 for misses. Results of the K-S tests are listed in Table 7.

In Figure 6, we show absorber Lyα equivalent width versus galaxy orientation angle and versus galaxy stellar mass. Pearson tests show no correlation between W and either ϕ or M_{*} at high significance.

5. Discussion

This study represents a truly blind survey of the CGM around galaxies by leveraging the extensive photometric data from SDSS in a way that targeted spectroscopic studies cannot. The COS-Halos sample (Tumlinson et al. 2013) probes the CGM within ∼150 kpc of 44 galaxies. Keeney et al. (2018) present extensive spectroscopic data for nearly 9000 galaxies in Mpc-scale fields of 47 QSOs, 90% complete to $L\sim0.1L^{*}$ for $z<0.1$. Here, we include over 10 times as many galaxies in similarly sized fields around each QSO in the sample, and with the photometry alone, we can reach similar completeness levels to $z\sim0.3$. Of course, this depth comes at the expense of precise redshift information, which is absolutely critical for establishing physical correspondences between galaxies and absorbers. In order to compensate, we have devised two Bayesian statistics, which build on the results of the previous targeted and detailed studies, and which in general reliably reproduce their results, within the parameters of our analysis.

The results of our Bayesian analysis show consistency in the sense that they are similar using either of the two statistics we developed: the virial radius method based on the empirical anticorrelation between absorption equivalent width in Lyα

Table 7
Galaxy–Lyα Absorber Pair Distribution

	D_{max}	P_{KS}
Unique Galaxy–Absorber Pairs		
$u-r>2.2$ versus $u-r<2.2$		
Virial Radius Method		
ρ	0.43	7.7×10^{-24}
W	0.10	0.12
Stellar Mass Method		
ρ	0.42	0.
W	0.11	0.067
$L/L^{*}<0.1$ versus $L/L^{*}>0.1$		
Virial Radius Method		
ρ	0.70	6.6×10^{-16}
W	0.15	8.7×10^{-4}
Stellar Mass Method		
ρ	0.69	1.8×10^{-74}
W	0.12	0.019
Hits versus Misses within 500 kpc		
Virial Radius Method		
ρ	0.20	1.6×10^{-8}
ρ[a]	0.26	8.2×10^{-5}
$u-r$	0.21	9.6×10^{-9}
$\log M_{*}/M_{\odot}$	0.21	4.4×10^{-9}
ϕ	0.04	0.65
Stellar Mass Method		
ρ	0.18	5.6×10^{-7}
ρ[a]	0.30	7.3×10^{-6}
$u-r$	0.20	1.9×10^{-8}
$\log M_{*}/M_{\odot}$	0.20	1.9×10^{-8}
ϕ	0.05	0.52

Note.
[a] Metal line systems.

and several metal species and galaxy–absorber impact parameter relative to galaxy virial radius, and the stellar mass method based on a scaling with galaxy stellar mass instead of virial radius. The specific SDSS galaxies paired with each COS absorber are usually the same, although specific differences can be found in Tables 4 and 5, and a few cases are outlined in the notes on individual sightlines in the Appendix. None of the relationships between the absorbers we identify as candidate CGM absorbers with galaxy properties that we investigated differed between the two methods, so the general conclusions we draw apply to both methods.

The candidate galaxy–absorber pairs identified through the virial radius method, shown on the W versus ρ/r_{vir} relation in Figure 2, cluster at $\rho=3-5r_{vir}$ and Lyα equivalent width $\sim$100 mÅ, weaker absorption than found in the literature for the spectroscopically identified pairs. The results of Keeney et al. (2018) suggest that the covering fraction is $\sim$60% or higher out to $4r_{vir}$, and Liang & Chen (2014) find the Lyα covering fraction is as high as 60% out to 500 kpc from the SDSS spectroscopic redshift sample, although Stocke et al. (2013) associate these "hits" falling outside galaxy virial radii as IGM rather than CGM.

There is a less pronounced tendency for $\rho>r_{vir}$ among metal line systems, consistent with the findings of Liang & Chen (2014), who report a sharp cutoff in metal line absorption for $\rho>200$ kpc, with lower ionization species declining more rapidly than higher ions like C IV, consistent with our fits to the literature data tabulated in Table 2. The candidate galaxy–absorber pairs found using the stellar mass method shown in Figure 3 are spread over a similar range of M_{*} found by the studies using spectroscopic galaxy redshifts.

Lanzetta et al. (1995) suggested that 30%–60% of the Lyα features in QSO spectra could arise in the CGM of luminous galaxies. By contrast, Stocke et al. (2013) find that only 5% of QSO sightlines pass within r_{vir} of a galaxy and are likely to be associated with the CGM, if the strict definition is gas within the virial radius. Of the $\sim$1450 Lyα absorption lines in the COS sample with significance level greater than four, we find that 57%–59% are uniquely paired with galaxies within our probability threshold, although only $\sim$6% lie along sightlines within r_{vir}, as shown in Figure 2. The $\sim$30%–40% false-positive rate for pairs with $\rho<r_{vir}$ places our estimate of the percentage of QSO absorbers arising in the CGM even lower for this SDSS sample, with a median $L\sim0.1L^{*}$.

Using all SDSS galaxies within 500 kpc of the sample QSOs and all the galaxy–absorber pairs in our ranked lists to estimate the Lyα covering fraction from the galaxy "hits" and "misses," we find the $f_c\sim0.61$ for all SDSS galaxies within $\rho/r_{vir}=3$, with no distinction between the lower-luminosity and higher-luminosity subsamples. This is a crude estimate, however, given the imprecision with which photometric redshifts allow us to establish velocity alignment between specific absorbers and galaxies. The estimate at higher impact parameters, $\rho/r_{vir}=3-6$, rises to $f_c\sim0.84$, reflecting the overall tendency of our method to identify pairs at larger impact parameter. Among the candidate galaxy–absorber pairs, we find that the impact parameter distribution is significantly different for galaxies of different color and luminosity, in the sense that there is a preference for absorption at larger impact parameters among bluer, lower-luminosity galaxies. This is consistent with Keeney et al. (2018), who find a shallower drop in the covering fraction for $L<L^{*}$, and higher covering fractions at $\rho=3-4r_{vir}$ for lower-luminosity, emission line galaxies. We also find a difference in the color distribution between galaxies within 500 kpc of QSO sightlines that show absorption ("hits") and those that do not ("misses"). There is a distinct preference for bluer galaxies among the hits—again, consistent with a tendency for star-forming galaxies to show a higher covering fraction.

The similarity of the galaxy orientation angle distributions between hits and misses, as well as the lack of any significant correlation between ϕ and W, are in agreement with previous results, e.g., Borthakur et al. (2015), who find that Lyα equivalent width does not correlate with orientation of the galaxy disk relative to the quasar sightline, indicating a spherical H I distribution in the CGM, and Pointon et al. (2019), who find no dependence of CGM metallicity on orientation angle.

Galaxy hits show a slight preference for larger impact parameter, which may indicate that we are probing group environments or large-scale structure (Tejos et al. 2014;

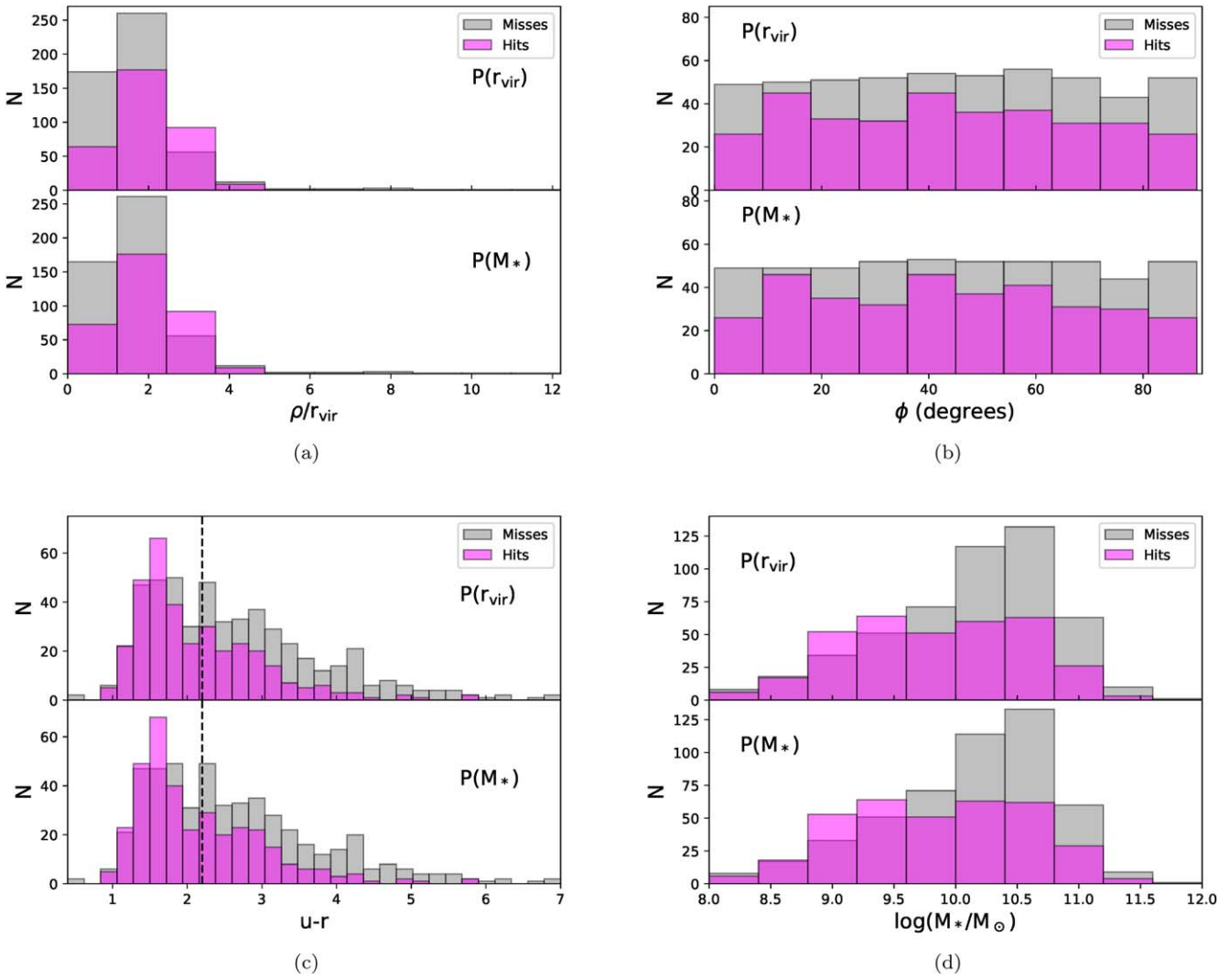

Figure 5. Distributions of galaxies paired with absorbers ("hits") and galaxies not paired with absorbers ("misses") within 500 kpc of the QSO sightlines: (a) galaxy–absorber impact parameter; (b) galaxy orientation angle; (c) galaxy $u - r$ color, where vertical dashed line at $u - r = 2.2$ is the boundary between early and late morphological types in the bimodal SDSS galaxy color distribution (Strateva et al. 2001); (d) galaxy stellar mass.

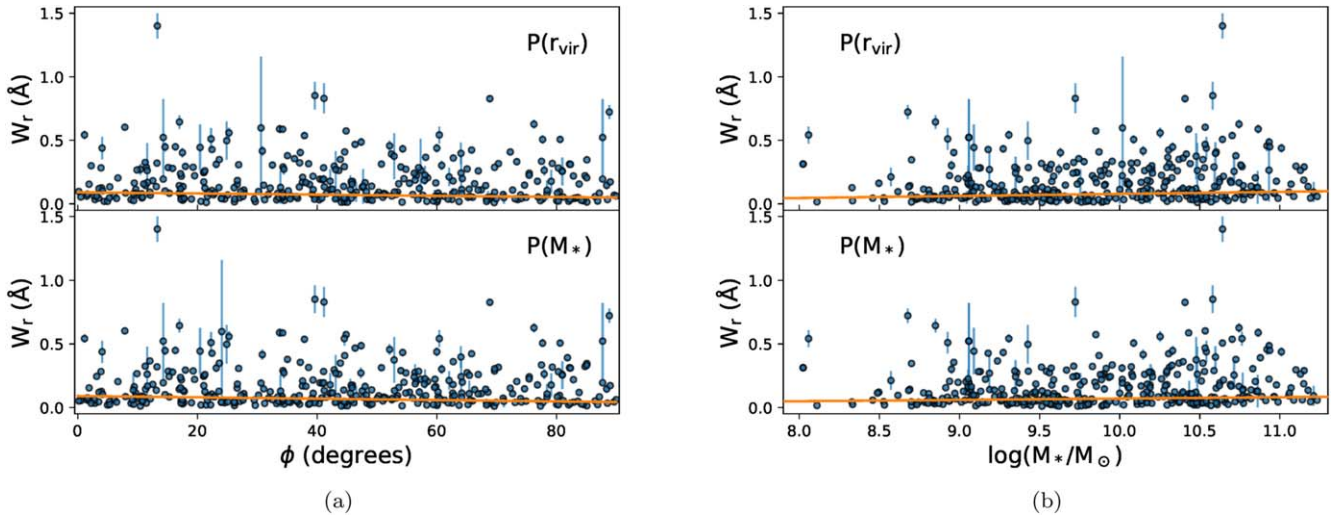

Figure 6. (a) Lyα rest equivalent width vs. galaxy orientation angle; (b) Lyα rest equivalent width vs. galaxy stellar mass.

Burchett et al. 2020; Wilde et al. 2021). However, metal line systems show the opposite preference, with hits tending to be found $\sim 0.7 r_{\rm vir}$ closer to QSO sightlines than misses. We also find a preference for absorption by smaller M_* galaxies, although we find no dependence of absorption equivalent width on stellar mass.

6. Summary

We present a method for using galaxy photometric redshifts combined with other CGM information in the literature to identify candidate galaxy–absorber pairs for follow-up spectroscopic confirmation. To develop this method, we use a sample of 43 HST/COS QSO spectra and the SDSS galaxy photometry in the QSO fields within 3° of the sightline. The photometric data are $>90\%$ complete to $L = 0.5L^*$ for $z = 0.5$, the maximum redshift we consider. Our basic results can be summarized as:

1. We find over 600 unique galaxy–absorber pairs using two different methods with median $\rho \sim 430$ kpc, including ∼85 pairs with metal line systems with median $\rho \sim 250$ kpc. Up to 75% of these pairs may be spurious due to misalignments between the photometric redshift estimates of the galaxies and their true redshifts, but results may be culled for higher-probability associations to establish samples for spectroscopic follow-up in some heretofore unsurveyed QSO fields.
2. Of the 47 galaxy–absorber pairs in the literature that are part of our SDSS galaxy sample, we recover ∼34 with our two statistics.
3. We discuss over 30 interesting individual potential galaxy–absorber pairs in the Appendix.
4. The galaxies identified as candidates for showing CGM absorption in the COS spectra with this method have the following median properties: $z_{\rm phot} = 0.13$, $M_r = -20.0$, $u - r = 1.7$, and $\log(M_*/M_\odot) = 9.7$.
5. The candidate galaxy–absorber pairs found here show a preference for larger impact parameter, bluer color, and lower stellar mass than unpaired SDSS galaxies within 500 kpc of the QSO sightlines, but no preference in orientation angle relative to the QSO sightline.
6. Among the galaxies paired with absorbers, there is a clear tendency for more luminous, redder galaxies to show absorption at lower impact parameter, within $4r_{\rm vir}$, and a more modest tendency for the absorbers in these pairs to show larger equivalent widths.

The authors thank the anonymous referee for helpful comments that improved the manuscript. This work was supported by National Science Foundation grant AST-0952923, and made extensive use of data from the Sloan Digital Sky Survey, SDSS-III. Funding for SDSS-III has been provided by the Alfred P. Sloan Foundation, the Participating Institutions, the National Science Foundation, and the U.S. Department of Energy Office of Science. The SDSS-III website is http://www.sdss3.org/. SDSS-III is managed by the Astrophysical Research Consortium for the Participating Institutions of the SDSS-III Collaboration including the University of Arizona, the Brazilian Participation Group, Brookhaven National Laboratory, Carnegie Mellon University, University of Florida, the French Participation Group, the German Participation Group, Harvard University, the Instituto de Astrofisica de Canarias, the Michigan State/Notre Dame/JINA Participation Group, Johns Hopkins University, Lawrence Berkeley National Laboratory, Max Planck Institute for Astrophysics, Max Planck Institute for Extraterrestrial Physics, New Mexico State University, New York University, Ohio State University, Pennsylvania State University, University of Portsmouth, Princeton University, the Spanish Participation Group, University of Tokyo, University of Utah, Vanderbilt University, University of Virginia, University of Washington, and Yale University. This work also used High Level Science Products provided by the Barbara A. Mikulski Archive for Space Telescopes under a Creative Commons Attribution license (CC BY 4.0); and the NASA/IPAC Extragalactic Database (NED), which is operated by the Jet Propulsion Laboratory, California Institute of Technology, under contract with the National Aeronautics and Space Administration.

Appendix
Notes on Individual QSO Sightlines

A.1. 1ES 1028+511

Stocke et al. (2013) found absorbing galaxies UGC 5740 and SDSS J103108.88+504708.7 with $(z_{\rm gal},\ \rho) = (0.002,\ 90$ kpc) and (0.003, 25 kpc), respectively. UGC 5740 is also matched by Stocke et al. (2013) to an absorber in the spectrum of 1SAX J1032.3+5051. These galaxies are not in our galaxy catalog, due to their very low redshifts and the photometric redshift error cut we applied. Instead, our formalism combines the $z_{\rm abs} = 0.0024$ and $z_{\rm abs} = 0.0032$ Lyα lines into one system and associates them with either SDSS J103541.06+500601.4, $(z_{\rm phot},\ \rho) = (0.021,\ 255$ kpc) or SDSS J103001.38+505047.5 $(z_{\rm phot},\ \rho) = (0.021,\ 50$ kpc). The SDSS spectroscopic redshift measurements of these galaxies are $z_{\rm gal} = 0.030$ and $z_{\rm gal} = 0.044$, respectively. Thus the pairings reported by Stocke et al. (2013) are more likely.

As tabulated in Table 6, Liang & Chen (2014) associate a Lyα absorption feature with a $z = 0.137274$ galaxy SDSS J103110.35+505211.0 at $\rho = 278.6$ kpc from the QSO sightline. We recover this pair as the top galaxy match for this absorber, which we associate with additional Lyα and O VI components. However, our uniqueness criteria pair this galaxy with a different absorber, listed in Tables 4 and 5, for which it is also the top match: a Lyα line with $z_{\rm abs} = 0.1406$.

Of the other potential galaxy–absorber pairs listed in these tables, we find a match of a $z_{\rm abs} = 0.051$ absorber with SDSS J103157.08+505753.2, $(z_{\rm phot},\ \rho) = (0.047,\ 447$ kpc). This galaxy is also matched, with similar single ion probabilities, to an absorption system in the spectrum of 1SAX J1032.3+5051. It is flagged as a nearby galaxy for both QSOs by Keeney et al. (2018).

A.2. 1ES1553+113

We report 27 (28) potential galaxy–absorber matches in Tables 4(5), including one O VI absorber $z_{\rm abs} = 0.395$ and galaxy with SDSS J123952.34+104515.1, $(z_{\rm phot},\ \rho) = (0.41,$ 189 kpc).

A.3. 1SAX J1032.3+5051

Stocke et al. (2013) reported an absorbing galaxy, UGC 5740, very close to the sightline at $\rho = 65$ kpc, with $z_{\rm gal} = 0.00216$ km s^{-1}. UGC 5740 is also matched by Stocke

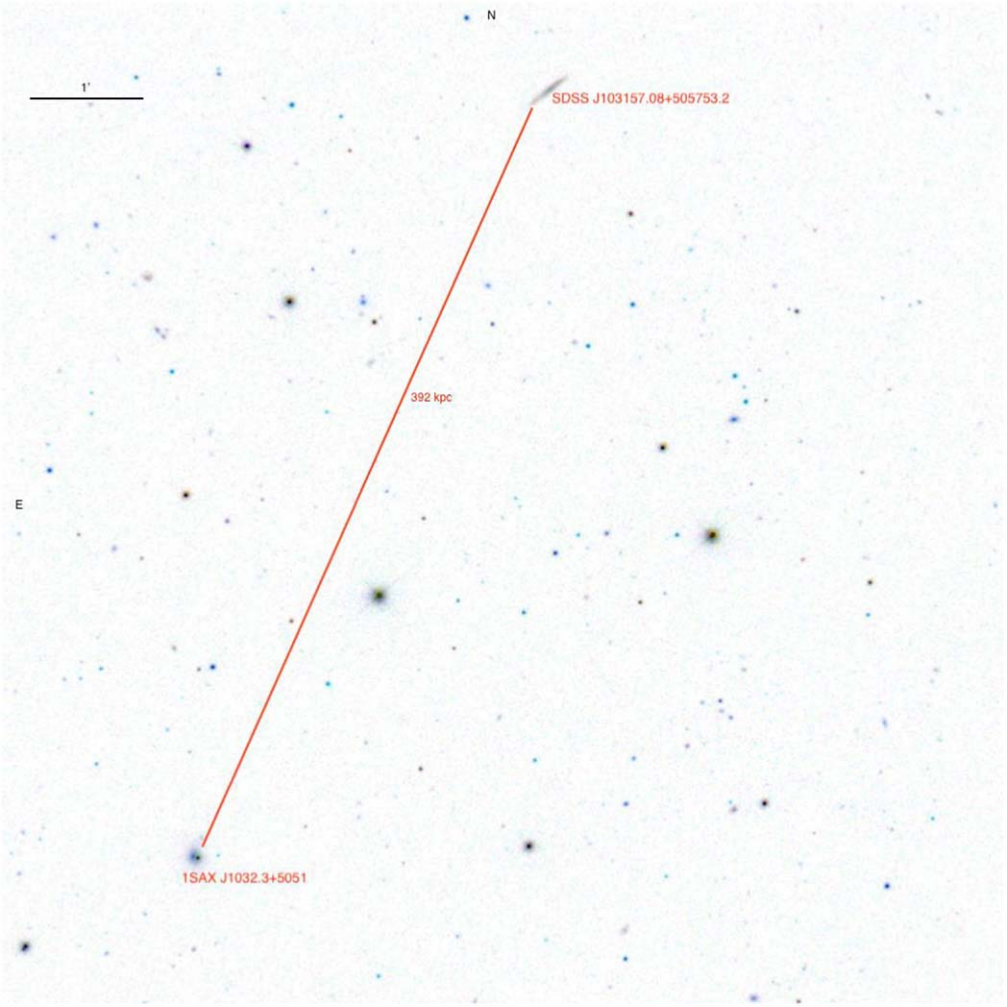

Figure 7. Galaxy SDSS J103157.08+505753.2, (z_{phot}, ρ) = (0.047, 392 kpc), paired with $z_{abs} = 0.045$ in the spectrum of 1SAX J1032.3+5051.

et al. (2013) to an absorber in the spectrum of 1ES 1028+511. As reported above, UGC 5740 is not in our SDSS galaxy catalog.

Instead, we find six other potential galaxy–absorber pairs, including a multicomponent absorption system (two Lyα components and a Si III line) paired with SDSS J103157.08 +505753.2, the galaxy also paired with an absorber in the spectrum of 1ES 1028+511, discussed above. It lies at $\rho = 392$ kpc from this sightline. The SDSS image is shown in Figure 7. This galaxy is flagged by Keeney et al. (2018) as a nearby galaxy, but not the closest known, to this absorber.

A.4. 3C 263

Liang & Chen (2014) report that the galaxy SDSS J114015.59+655551.7 ($\rho = 456$ kpc) is not matched with any absorber in the QSO spectrum. We do find a three-component $z_{abs} = 0.046$ Lyα absorber paired to this galaxy. Its spectroscopic redshift, $z_{gal} = 0.04588$, is in even better agreement with z_{abs} than the photometric estimate, $z_{phot} = 0.050$.

A $z_{abs} = 0.063$ system with three Lyα components, as well as one Si II, two Si III, one Si IV, one C II, and two C IV components is matched with SDSS J114005.17+654801.3 with $\rho = 63$ kpc and $z_{phot} = 0.093$ is flagged by Keeney et al. (2018) as the closest known galaxy to this absorber. The stellar mass method instead pairs this galaxy with a different multicomponent metal line system with $z_{abs} = 0.113$, at $\rho = 107$ kpc.

We find 23 other possible galaxy–absorber pairs for this QSO sightline from both methods, including a $z_{abs} = 0.11$ system with Lyα, O VI, C IV, and Si III components paired with SDSS J113956.96+654459.6 (z_{phot}, $\rho = 0.11$, 353 kpc) by the virial radius method and with SDSS J114005.17+654801.3 (z_{phot}, $\rho = 0.093$, 107 kpc) by the stellar mass method. Both galaxies are flagged by Keeney et al. (2018) as being the closest known galaxies to absorbers.

A.5. 3C 273

This sightline passes through the Virgo cluster. The galaxy H I 1225+01 lies at $\rho = 126$ kpc from the QSO sightline. Bowen et al. (1996) associate it with $z_{abs} = 0.004$ Lyα absorption in the HST Faint Object Spectrograph data, and Penton et al. (2002) note its coincidence with $z_{abs} = 0.00337$ and $z_{abs} = 0.00527$ features in the spectrum taken by the Goddard High Resolution Spectrograph. This galaxy is not in our SDSS sample, due to its low redshift and the photometric redshift error cut we applied.

The following absorption systems are matched to galaxies by various authors:

1. $z_{abs} = 0.0034$: The galaxies in this region may reside in a group environment (Stocke et al. 2013). Bowen et al. (1996), Penton et al. (2002), and Stocke et al. (2013) note the coincidence of this absorber to SDSS J123103.89 +014034.4, with $z_{gal} = 0.00368$, at $\rho = 118$ kpc from the line of sight. This galaxy is not in our SDSS sample, due to the photometric redshift error cut. Liang & Chen (2014) associate this absorber with SDSS J122815.96 +014944.1, $(z_{gal}, \rho) = (0.00303, 69$ kpc). We do recover this match with both methods. However, because the photometric redshift for this galaxy, $z_{phot} = 0.013$, is not in good agreement with the spectroscopic value, we find $P(r_{vir}) = P(M_*) = 0.13$, and its unique match is to a different Lyα absorber: $z_{abs} = 0.020$, $\rho = 472$ kpc, with $P(r_{vir})$, $P(M_*) = 0.26$, 0.29. Our statistics match the $z_{abs} = 0.0034$ absorber instead to SDSS J122806.95 +032056.2, $(z_{phot}, \rho) = (0.012, 377$ kpc), with a probability close to our 10% threshold value. Given the spectroscopic redshift information available for SDSS J122815.96+014944.1 and used in the analysis of Liang & Chen (2014), we consider its association with the $z_{abs} = 0.0034$ absorber to be most plausible.
2. $z_{abs} = 0.0053$: Absorption at this redshift is linked to two different galaxies in this likely group environment by Stocke et al. (2013): NGC 4420 and SDSS J122950.57 +020153.7. The former is not in our SDSS catalog, due to our magnitude cut. The latter is assigned a photometric redshift of 0.036, so it is not among the top 10 probable galaxy matches to this absorber using either of our two statistics. Our two methods find no unique galaxy matches to this absorber.
3. $z_{abs} = 0.0072$, 0.0075: Penton et al. (2002) and Wakker & Savage (2009) match the $z_{abs} = 0.0072$ absorber to UGC 7625, at a fairly large impact parameter to the line of sight, 771 kpc, and also to absorption in the Q1230 +0115 sightline, with $\rho = 339$ kpc. This galaxy is not in our SDSS catalog, due to our photometric redshift error cut. Wakker & Savage (2009) match the $z_{abs} = 0.0075$ absorber to SDSS J122815.88+024202.9 $(z_{gal}, \rho) = (0.00762, 429$ kpc). In the methodology presented here, the two absorbers are combined into one system, and since UGC 7625 is absent from our catalog, SDSS J122815.88+024202.9 is the top match to the absorber for both methods, even though the photometric redshift of the galaxy, $z_{phot} = 0.019$, is in poor agreement with z_{abs} and with the spectroscopic value reported by SDSS, $z_{phot} = 0.0074$.

We report 25 other possible galaxy–absorber pairs along this sightline with both methods, including an O VI absorber with $z_{abs} = 0.12$ paired with SDSS J122910.05+020120.1, $(z_{phot}, \rho) = (0.125, 24$ kpc) by both methods.

A.6. FBQS 1010+3003

Stocke et al. (2013) report an association of a $z_{abs} = 0.00462$ absorber with the galaxy UGC 5478 $(z_{gal}, \rho) = (0.00459, 48$ kpc). This galaxy is not in our SDSS catalog, due to the photometric redshift error cut. Our best unique match to this absorber, SDSS J101042.80+293136.7, $(z_{phot}, \rho) = (0.019, 191$ kpc), has a rather poor redshift agreement, and so we would not choose this over UGC 5478 as the most likely galaxy associated with this system.

Liang & Chen (2014) find that the $z_{abs} = 0.0875$ absorber is associated with SDSS J101008.85+300252.5 $(z_{gal}, \rho) = (0.0874, 181$ kpc). Because the SDSS photometric redshift estimate for this galaxy is 0.111, it is the seventh-best match for this absorber with our methods. Both methods find that the galaxy SDSS J100950.99 +300703.0, $(z_{phot}, \rho) = (0.091, 392$ kpc), is the best match for this absorber. The galaxy has no spectroscopically measured redshift.

We report 18 (17) other unique galaxy–absorber pairs for this sightline from the virial radius(stellar mass) method. The highest-probability pairs are: $z_{abs} = 0.082$ and SDSS J100940.28 +300640.9, $(z_{phot}, \rho) = (0.083, 490$ kpc); $z_{abs} = 0.155$ and SDSS J101006.14+300613.8, $(z_{phot}, \rho) = (0.15, 479$ kpc); $z_{abs} = 0.25$ and SDSS J101003.92+300141.6, $(z_{phot}, \rho) = (0.25, 491$ kpc). However, the relatively large impact parameters and the SDSS spectroscopic redshift for SDSS J100940.28+300640.9, $z_{gal} = 0.094$, throw these matches into some question.

A.7. HS 1102+3441

We find 19 possible pairs with the virial radius method, 18 with the stellar mass method. Of these paired absorbers, five are metal line systems:

1. $z_{abs} = 0.201$, matched with SDSS J110534.38+342403.5, $(z_{phot}, \rho) = (0.20, 377$ kpc);
2. $z_{abs} = 0.205$, matched with SDSS J110546.32+342721.2, $(z_{phot}, \rho) = (0.25, 457$ kpc);
3. $z_{abs} = 0.238$, matched with SDSS J110539.49+342653.8, $(z_{phot}, \rho) = (0.22, 303$ kpc);
4. $z_{abs} = 0.289$, matched with SDSS J110540.90+342514.9, $(z_{phot}, \rho) = (0.26, 104$ kpc); and
5. $z_{abs} = 0.408$, matched with SDSS J110537.33+342535.9, $(z_{phot}, \rho) = (0.38, 168$ kpc).

None of these galaxies has a spectroscopically confirmed redshift, and plausible associations would require better agreement with the absorber redshifts in most cases. None of the galaxy pairings we find for the absorbers in this sightline overlaps with the spectroscopic sample of Keeney et al. (2018).

A.8. MRK 106

There are two galaxy–absorber pairs for this sightline reported in the literature. Wakker & Savage (2009) match the $z_{abs} = 0.00811$ absorber with SDSS J091923.29+553137.2, and Liang & Chen (2014) pair the $z_{abs} = 0.0317$ absorber with UGC 4800. Neither of these galaxies are in our SDSS galaxy catalog, due to the photometric redshift error cut. Also, UGC 4800 lies at a projected distance of 1030 kpc, larger than the maximum of 500 kpc that we imposed. We report 9 (7) possible galaxy–absorber pairs for this sightline from the virial radius (stellar mass) method. The highest-probability matches are to two Lyα absorbers: $z_{abs} = 0.008$ paired with SDSS J092000.79+554635.2, $(z_{phot}, \rho) = (0.011, 248$ kpc); and $z_{abs} = 0.038$ matched to SDSS J092030.67+553102.2, $(z_{phot}, \rho) = (0.032, 487$ kpc). The latter is is unlikely, given the galaxy's SDSS spectroscopic redshift, $z_{gal} = 0.046$.

A.9. MRK 1513

We find only three (four) unique galaxy–absorber pairs in this field with the virial radius (stellar mass) method, all with $\rho > 400$ kpc.

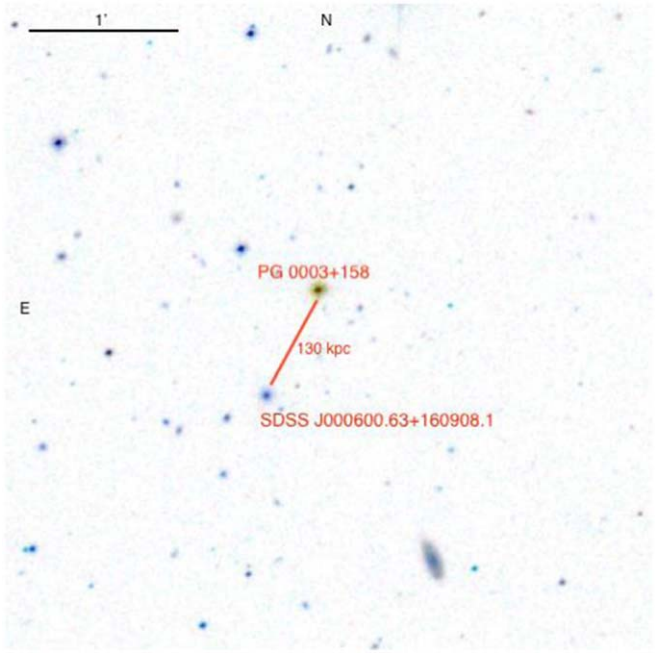

Figure 8. Galaxy SDSS J000600.63+160908.1, ($z_{\rm phot}$, ρ) = (0.16, 130 kpc), paired with $z_{\rm abs} = 0.165$ in the PG 0003+158 spectrum.

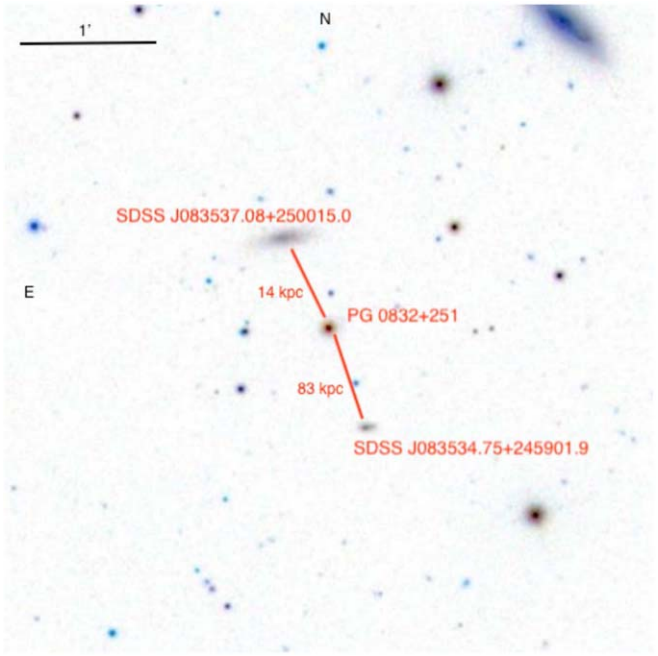

Figure 9. Galaxy SDSS J083537.08+250015.0, ($z_{\rm phot}$, ρ) = (0.031, 14 kpc), paired with $z_{\rm abs} = 0.0174$ in the spectrum of PG 0832+251; and galaxy SDSS J083534.75+245901.9, ($z_{\rm phot}$, ρ) = (0.098, 83 kpc), paired with $z_{\rm abs} = 0.108$.

A.10. MRK 478

Wakker & Savage (2009) associate an absorber with $z_{\rm abs} = 0.00525$ with the galaxy NGC 5727 ($\rho = 645$ kpc). The photometric redshift estimate for this galaxy, 0.198, is in poor agreement with the spectroscopic value, $z_{\rm gal} = 0.00497$, and its impact parameter is larger than our 500 kpc upper limit, so we do not find this galaxy in our top 10 matches to this absorber. Both methods find the top match to this absorber is SDSS J143800.57+360124.2, ($z_{\rm phot}$, ρ) = (0.018, 401 kpc), and identify two other possible galaxy–absorber pairs.

A.11. PG 0003+158

Liang & Chen (2014) report a galaxy–absorber pair for $z_{\rm abs} = 0.0909$ and SDSS J000556.15+160804.1 ($\rho = 193$ kpc). This galaxy is identified as the highest-probability unique match to the five-component absorber (three Lyα, two C IV) with both methods.

The virial radius (stellar mass) method reveals 22 (25) other possible galaxy–absorber pairs, including a $z_{\rm abs} = 0.165$ system with Lyα, O VI, and C III, paired with SDSS J000600.63+160908.1, ($z_{\rm phot}$, ρ) = (0.16, 130 kpc). The spectroscopic redshift is in excellent agreement, $z_{\rm gal} = 0.165$, strengthening the conclusion of a physical association. This galaxy is shown in Figure 8.

We also pair a five-component $z_{\rm abs} = 0.347$ system showing three Lyα, two O VI, C III, and Si II components with the galaxy SDSS J000601.78+160837.7, ($z_{\rm phot}$, ρ) = (0.34, 398 kpc).

A.12. PG 0026+129

Bowen et al. (1997) match a $z_{\rm abs} = 0.0391$ absorber to the galaxy WISEA J002915.37+132056.5 ($\rho = 111$ kpc). Because $z_{\rm phot} = 0.028$, this galaxy is identified as the second-best match for this absorber with our methods. Instead, this galaxy is paired with a $z_{\rm abs} = 0.033$ Lyα absorber after uniqueness is imposed. The top galaxy match to the $z_{\rm abs} = 0.0391$ absorber in both methods is SDSS J002843.85+131421.4, ($z_{\rm phot}$, ρ) = (0.031, 348 kpc). The virial radius (stellar mass) method identifies five (four) additional possible galaxy–absorber pairs listed in Tables 4 and 5.

A.13. PG 0157+001

This sightline has no previously reported galaxy–absorber pairs. Both methods find 12 potential pairs, including a multicomponent absorber with two Lyα components and one Si III with $z_{\rm abs} = 0.146$ and the galaxy SDSS J015946.54+002320.5, ($z_{\rm phot}$, ρ) = (0.158, 153 kpc). However, the spectroscopic redshift of this galaxy, $z_{\rm gal} = 0.161$, suggests that, if the absorber is circumgalactic in origin, it likely arises from another galaxy.

A.14. PG 0832+251

Liang & Chen (2014) identify a $z_{\rm abs} = 0.0073$ system with SDSS J083335.65+250847.1 ($\rho = 263$ kpc). The SDSS photometric redshift cut removes this galaxy from our catalog. Stocke et al. (2013) find an association between $z_{\rm abs} = 0.0174$ and NGC 2611, at $\rho = 53$ kpc from the QSO line of sight. We recover this galaxy as the second match for the virial radius method and the top match for the stellar mass method, even though its SDSS photometric redshift estimate, $z_{\rm phot} = 0.026$, is not in good agreement with the absorber redshift. Interestingly, our top match from the virial radius method yielded a different galaxy, SDSS J083537.08+250015.0, with ($z_{\rm phot}$, ρ) = (0.031, 14 kpc). The spectroscopic redshift, $z_{\rm gal} = 0.017$, places it in even better agreement with $z_{\rm abs}$. Its even closer proximity to the QSO sightline merits follow-up investigation. This pair is shown in Figure 9.

Liang & Chen (2014) pair a $z_{\rm abs} = 0.0233$ absorber with SDSS J083607.41+250645.7 ($\rho = 283$ kpc), and Keeney et al.

(2018) flag this galaxy as the closest known galaxy to the absorber. The SDSS photometric redshift of this galaxy is in good agreement with the spectroscopic value and with z_{abs}. Both methods find this to be the second-best galaxy match. The top galaxy match is SDSS J083645.44+250652.0, (z_{phot}, ρ) = (0.021, 492 kpc). However, the galaxy's spectroscopic redshift, $z_{gal} = 0.026$, rules it out. Our methods instead pair SDSS J083607.41+250645.7 with a double Lyα component system with $z_{abs} = 0.028$ and $\rho = 343$ kpc. Given the spectroscopic redshift, we favor the galaxy–absorber pair for $z_{abs} = 0.023$ found by Liang & Chen (2014).

Our methods identify 16 additional galaxy–absorber pairs with the two methods. We find two Lyα lines with $z_{abs} = 0.101$ paired with SDSS J083531.17+245548.7, (z_{phot}, ρ) = (0.10, 453 kpc) and an O VI absorber with $z_{abs} = 0.233$ paired with SDSS J083535.75+250032.9, (z_{phot}, ρ) = (0.25, 194 kpc). However, Keeney et al. (2018) find no absorber within 1000 km s^{-1} of these galaxies.

Finally a Lyα absorber with $z_{abs} = 0.108$ is matched to SDSS J083534.75+245901.9 with (z_{phot}, ρ) = (0.098, 83 kpc). The galaxy is flagged as the closest to this absorber by Keeney et al. (2018). This pair is also shown in Figure 9.

A.15. PG 0844+349

Wakker & Savage (2009) find associations between absorbers with $z_{abs} = 0.00137$ and $z_{abs} = 0.00769$ with NGC 2683 and UGC 4621, respectively. These two galaxies are too bright to be in our SDSS galaxy catalog. The virial radius (stellar mass) method yields three (two) candidate galaxy–absorber pairs with probability greater than our 10% threshold.

A.16. PG 0953+414

Wakker & Savage (2009) pair a $z_{abs} = 0.00204$ absorber with NGC 3104 a galaxy with the same redshift and an impact parameter of 296 kpc from the sightline. This galaxy is too bright to be part of our SDSS galaxy sample. Instead, our methods pair this absorber with SDSS J094758.66+412057.7 (z_{phot}, ρ) = (0.015, 296 kpc).

Stocke et al. (2013) and Liang & Chen (2014) identify a pairing of $z_{abs} = 0.142$ with SDSS J095638.90+411646.0, at $\rho = 435$ kpc. This galaxy's photometric redshift estimate is $z_{phot} = 0.131$, and without the reliable spectroscopic redshift information, it is the seventh-best match for the absorber in our virial radius method. It is the third-best in the stellar mass method, and our uniqueness criteria do recover this galaxy–absorber pair in Table 5. Instead, the galaxy uniquely matched to this absorber by the virial radius method is SDSS J095706.09+411707.8, (z_{phot}, ρ) = (0.16, 473 kpc).

We report 16 (18) other possible galaxy–absorber pairs from the virial radius (stellar mass) method, including a $z_{abs} = 0.068$ C IV system matched to SDSS J095640.12+411107.6 with (z_{phot}, ρ) = (0.083, 380 kpc). However, this galaxy's spectroscopic redshift is reported by SDSS to be $z_{gal} = 0.041$.

A.17. PG 1001+291

This sightline has several galaxy–absorber pairs reported in the literature. The following are not reproduced by our methods because the galaxy is excluded from our SDSS galaxy catalog for the reasons listed in in Table 6: UGC 5427 and $z_{abs} = 0.00165$ (Wakker & Savage 2009); SDSS J100618.16 +285641.9 and $z_{abs} = 0.0036$ (Bowen et al. 1997; Liang & Chen 2014); SDSS J100402.36+285512.5 and $z_{abs} = 0.137$; and TON0028:[KSS94] 39 and $z_{abs} = 0.214$ (Mathes et al. 2014).

Our methods match the $z_{abs} = 0.00165$ absorber with SDSS J100534.47+273051.7 (z_{phot}, ρ) = (0.014, 180 kpc), but this is ruled out by its spectroscopic redshift, $z_{gal} = 0.0212$.

Two other galaxies paired with absorbers in this sightline by Wakker & Savage (2009) are included in our catalog: UGC 5464 and UGC 5461, paired with $z_{abs} = 0.00357$ and $z_{abs} = 0.0153$, respectively. This is a different galaxy match to the $z_{abs} = 0.00357$ absorber mentioned above. Neither of the these galaxies are recovered as unique matches to the absorbers with our methods, due to the inaccuracies of the photometric redshifts, estimated to be 0.0236 and 0.035. Additionally, UGC 5461 lies at an impact parameter larger than our 500 kpc limit. Instead, our methods match $z_{abs} = 0.00357$ with SDSS J100223.17+294333.3, (z_{phot}, ρ) = (0.014, 234 kpc), which is plausible given its reported spectroscopic redshift, $z_{gal} = 0.00274$. The $z_{abs} = 0.0153$ absorber is matched with SDSS J100427.09+284043.9 (z_{phot}, ρ) = (0.020, 298 kpc) by both methods, but the spectroscopic redshift is in good agreement with the photometric estimate, which is actually in rather poor agreement with the absorber redshift, so this match is unlikely.

Both methods do find that SDSS J100403.24+285650.2 is the top match to $z_{abs} = 0.134$, (z_{phot}, ρ) = (0.143, 181 kpc), as reported by Liang & Chen (2014). Because the photometric redshift is larger than the spectroscopically measured value, the probability of this galaxy matching with $z_{abs} = 0.137$ ($\rho = 185$ kpc) is found to be higher by both methods. This absorption system consists of two Lyα and one O VI components. However, given the spectroscopic information, we judge that this galaxy is more likely to be physically associated with $z_{abs} = 0.134$.

The methods find 11 additional potential pairs, including a double Lyα system with $z_{abs} = 0.165$ and the galaxy SDSS J100352.49+285508.9, (z_{phot}, ρ) = (0.162, 385 kpc).

A.18. PG 1048+342

Liang & Chen (2014) pair a $z_{abs} = 0.0593$ absorber with SDSS J105111.41+335935.6, at $\rho = 465$ kpc. The photometric redshift is in good agreement with the spectroscopic value and this pair is recovered with both methods.

Both methods result in seven additional matches, including a multicomponent $z_{abs} = 0.005$ absorber with three Lyα and two Si IV components matched with SDSS J105338.41+340159.4, (z_{phot}, ρ) = (0.011,,190 kpc). The spectroscopic redshift, $z_{gal} = 0.006$, strengthens the case. This pair is shown in Figure 10.

A.19. PG 1049-005

We find no previously reported specific galaxy–absorber pairs for this sightline. Our virial radius and stellar mass methods identify 17 and 16 possible pairs respectively. Two paired absorption systems show Lyα and Si III components: $z_{abs} = 0.038$ (Richter et al. 2016) is matched with SDSS J105147.77–005020.3, with (z_{phot}, ρ) = (0.040, 61 kpc) and spectroscopic redshift $z_{gal} = 0.038$; and $z_{abs} = 0.171$ is matched with SDSS J105147.68–005203.4, (z_{phot}, ρ) = (0.17, 214 kpc).

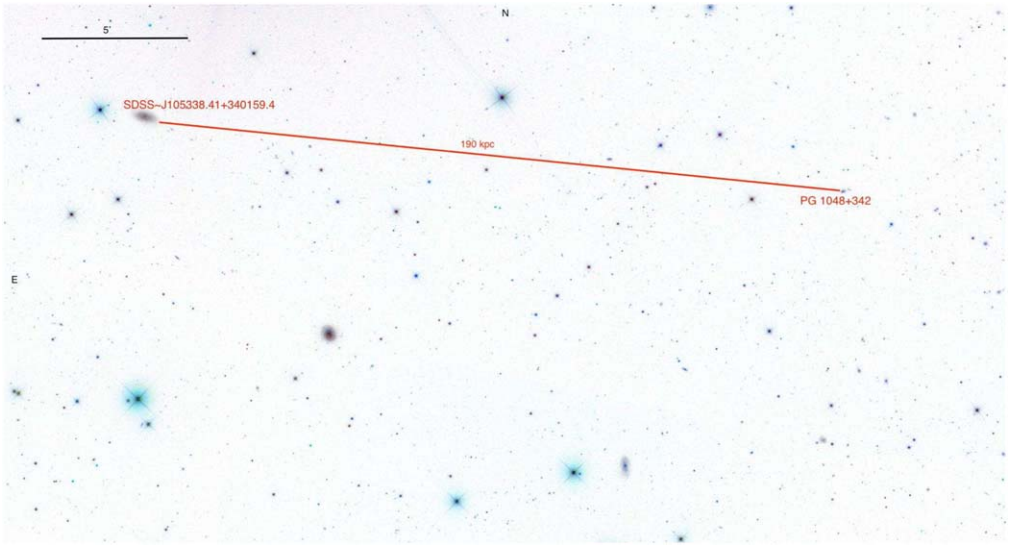

Figure 10. Galaxy SDSS J105338.41+340159.4, ($z_{\rm phot}$, ρ) = (0.011, 190 kpc), paired with $z_{\rm abs} = 0.005$ absorber in the spectrum of PG 1048+342.

A.20. PG 1115+407

Our methods find 11 possible galaxy–absorber pairs along this sightline. A two Lyα and two O VI component system with $z_{\rm abs} = 0.12$ is paired with SDSS J111814.91+402343.3, ($z_{\rm phot}$, ρ) = (0.11, 487 kpc) with both methods. Five other galaxy–absorber pairs found by our methods are flagged by Keeney et al. (2018) as the closest galaxy to an absorber, including the pairing of a $z_{\rm abs} = 0.12$ Lyα system with SDSS J111817.93+402612.0, ($z_{\rm phot}$, ρ) = (0.12, 328 kpc) and the pairing of a $z_{\rm abs} = 0.13$ O VI system with SDSS J111816.46+402505.6, ($z_{\rm phot}$, ρ) = (0.13, 388 kpc). Both are shown in Figure 11.

A.21. PG 1116+215

This sightline has a plethora of possible galaxy–absorber pairs presented in the literature, several of which we do not recover:

1. $z_{\rm abs} = 0.00493$, UGC 6258 (Wakker & Savage 2009): We do not recover this pair with either method, primarily due to the fact that its projected distance, 543 kpc, is larger than our threshold of 500 kpc. Instead, our methods match this absorber with SDSS J111349.11+213101.3, ($z_{\rm phot}$, ρ) = (0.010, 465 kpc).
2. $z_{\rm abs} = 0.0163$, NGC 3649 (Wakker & Savage 2009): This galaxy is excluded from our SDSS galaxy catalog, due to the photometric redshift error cut. Instead, we find a match with SDSS J111844.37+213351.0, with ($z_{\rm phot}$, ρ) = (0.017, 313 kpc). The spectroscopic redshift, $z_{\rm gal} = 0.0212$, calls this into question, however, so NGC 3649 is a more likely association.
3. $z_{\rm abs} = 0.0195$, SDSS J112045.94+211115.3 (Tripp et al. 1998): We do not recover this pair with either method, primarily due to the fact that its projected distance, 557 kpc, is larger than our threshold of 500 kpc. Our methods find no unique match for this absorber, i.e., the top galaxy match satisfying $P > 0.10$ is assigned to other absorbers. In fact, the algorithms find the top match for this absorber to be SDSS J111844.37+213351.0, and its spectroscopic redshift, $z_{\rm gal} = 0.021$, is in better agreement with this absorber than with the $z_{\rm abs} = 0.0163$ absorber it was uniquely matched with based on its $z_{\rm phot}$, which equals 0.018.
4. $z_{\rm abs} = 0.0322$, SDSS J111843.28+212723.0 (Liang & Chen 2014): Both methods recover this galaxy–absorber pair as the top galaxy match for this absorber. However, after the uniqueness criteria are applied, the galaxy paired with this absorber is SDSS J111833.63+211300.4, ($z_{\rm phot}$, ρ) = (0.039, 400 kpc), and SDSS J111843.28+212723.0 is instead paired with $z_{\rm abs} = 0.041$ ($\rho = 495$ kpc). Since the SDSS spectroscopic redshifts of SDSS J111843.28+212723.0 and SDSS J111833.63+211300.4, are $z_{\rm gal} = 0.0323$ and $z_{\rm gal} = 0.0601$, respectively, we consider the match reported by Liang & Chen (2014) to be the most plausible.

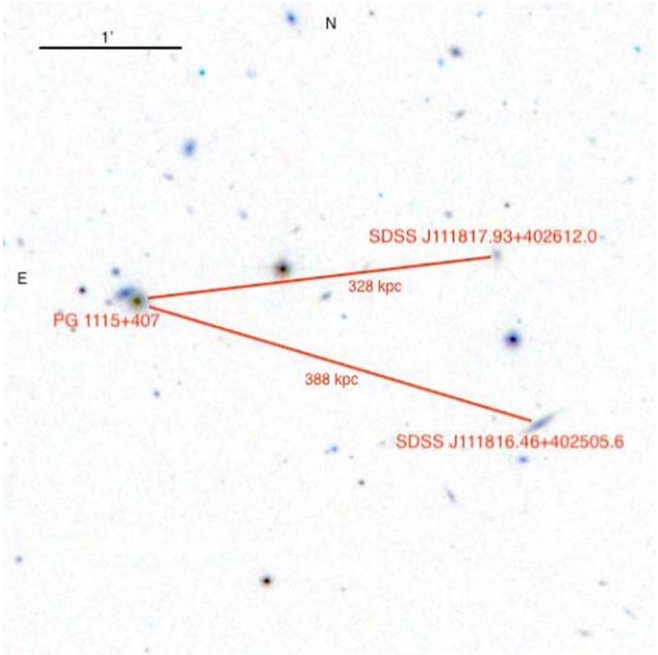

Figure 11. Galaxy SDSS J111817.93+402612.0, ($z_{\rm phot}$, ρ) = (0.12, 328 kpc), paired with a $z_{\rm abs} = 0.12$ Lyα system; and galaxy SDSS J111816.46+402505.6, ($z_{\rm phot}$, ρ) = (0.13, 388 kpc), paired with a $z_{\rm abs} = 0.13$ O VI absorber in the spectrum of PG1115+407.

5. $z_{abs} = 0.0412$, SDSS J111909.56+210243.4 (Tripp et al. 1998): We do not recover this pair with either method, primarily due to the fact that its projected distance, 746 kpc, is larger than our threshold of 500 kpc. The galaxy found to be the most probable match to this absorber by both methods is SDSS J111843.28+212723.0, uniquely identified with $z_{abs} = 0.0322$ as noted above.
6. $z_{abs} = 0.0590$, SDSS J111924.26+211029.9 (Tripp et al. 1998): We do not recover this pair with either method, primarily due to the fact that its projected distance, 601 kpc, is larger than our threshold of 500 kpc. Instead, our top match for this absorber is SDSS J111848.70+211441.4, $(z_{phot}, \rho) = (0.058, 450$ kpc). This galaxy is flagged by Keeney et al. (2018) as the closest to an absorber but not this absorber, as the galaxy's spectroscopic redshift is reported to be $z_{gal} = 0.041$. Thus, it is more likely a match to the $z_{abs} = 0.0412$ system discussed above.
7. $z_{abs} = 0.0590$, SDSS J111905.34+211537.7, SDSS J111905.51+211733.0 (Stocke et al. 2013): SDSS J111905.34+211537.7 is the seventh (sixth) best match to this absorber with the virial radius(stellar mass) method. SDSS J111905.51+211733.0 is the 10th-best match for the stellar mass method, and not in the top 10 highest probability galaxy matches with the virial radius method. Both methods pair this absorber instead with SDSS J111848.70+211441.4, $(z_{phot}, \rho) = (0.058, 450$ kpc), as noted above.
8. $z_{abs} = 0.0608$, SDSS J111942.04+212610.3 (Tripp et al. 1998): We do not recover this pair with either method, primarily due to the fact that its projected distance, 677 kpc, is larger than our threshold of 500 kpc.
9. $z_{abs} = 0.138$, SDSS J111906.68+211828.7 (Liang & Chen 2014): This is a multicomponent absorber with Si II, Si III, Si IV, C II, C IV, and Lyα. The galaxy's photometric redshift estimate, $z_{phot} = 0.134$, is in reasonable agreement with the spectroscopic redshift, so this match is recovered with both methods.

A.22. PG 1121+422

Liang & Chen (2014) report two galaxies associated with absorbers in this QSO sightline: SDSS J112418.74+420323.1 and $z_{abs} = 0.0245$, with an impact parameter of 123 kpc, and SDSS J112457.15+420550.8 and $z_{abs} = 0.0338$ with $\rho =$ 213 kpc. Our methods both recover the former as the unique galaxy match. The methods find the latter as the second-best galaxy match for the absorber, since $z_{phot} = 0.042$. The top match for this absorber is also SDSS J112418.74+420323.1, and so we report no unique galaxy match for $z_{abs} = 0.0338$ with $P > 0.10$.

The virial radius (stellar mass) method finds 12 (9) other possible galaxy–absorber pairs for this line of sight. We find a match between a $z_{abs} = 0.192$ metal line system with C II, Si II, C III, Si III, and O VI components and the galaxy SDSS J112433.82+420152.3, $(z_{phot}, \rho) = (0.175, 194$ kpc).

A.23. PG 1216+069

This Virgo cluster sightline has several galaxy–absorber associations reported in the literature, primarily from Bowen et al. (1996) using HST/Faint Object Spectrograph data. These authors associate one strong $z_{abs} = 0.00550$ absorber with 11 different possible galaxies. In the COS spectrum, this system shows four components, Lyα, two Si II lines, and one C II line, with $z_{abs} = 0.0061$–0.0063:

1. VCC 381, $z_{gal} = 0.00160$: This galaxy is excluded from our SDSS galaxy catalog, due to the photometric redshift error cut.
2. VCC 538, $z_{gal} = 0.00167$: The SDSS photometric redshift estimate for this galaxy is 0.384, so it is not in the top 10 matches to this absorber for either method.
3. IC 3115, $z_{gal} = 0.00244$: This galaxy is excluded from our SDSS galaxy catalog, due to our magnitude cut of $r < 14$.
4. VCC 446, $z_{gal} = 0.00283$: This galaxy, with $z_{phot} = 0.0128$, is the ninth-best match to the $z_{abs} = 0.0063$ absorber for the virial radius method, but is not in the top 10 matches with the stellar mass method.
5. UGC 7423, $z_{gal} = 0.00419$: The SDSS photometric redshift estimate for this galaxy is 0.0243, and it is not in the top 10 matches to this absorber for either method.
6. VCC 340, $z_{gal} = 0.00504$: This galaxy, with $z_{phot} = 0.0116$, is the 10th-best match to the absorber for the virial radius method, but is not in the top 10 matches with the stellar mass method.
7. VCC 329, $z_{gal} = 0.00541$: The SDSS photometric redshift estimate for this galaxy is 0.0913, and it is not in the top 10 matches to this absorber for either method.
8. NGC 4260, $z_{gal} = 0.00653$: This galaxy is excluded from our SDSS galaxy catalog due to our magnitude cut of $r < 14$.
9. VCC 223, $z_{gal} = 0.00690$: The SDSS photometric redshift for this galaxy is estimated at 0.0159. Thus, it is not in the top 10 matches to this absorber with either method.
10. NGC 4241, $z_{gal} = 0.00745$: This galaxy is excluded from our SDSS galaxy catalog, due to our magnitude cut of $r < 14$.
11. VCC 415, $z_{gal} = 0.00854$: This galaxy is excluded from our SDSS galaxy catalog, due to the photometric redshift error cut.

For this absorber, our virial radius method identifies the highest-probability unique match to be SDSS J121920.67+064218.4, $(z_{phot}, \rho) = (0.03, 28$ kpc). This is also the fourth top match for the stellar mass method. The spectroscopic redshift of this galaxy is $z_{gal} = 0.00741$, within $\sim$400 km s^{-1} of the absorber. The very small impact parameter is consistent with the large, 2.8 Å Lyα equivalent width. The second top match from the stellar mass method is SDSS J121838.62+064230.1, $(z_{phot}, \rho) = (0.019, 88$ kpc). It is not reported in Table 5, because $P_{ion} < 0.10$ for the Lyα component. (Similarly for the top match to this absorber, SDSS J121912.37+062253.6, $(z_{phot}, \rho) = (0.016, 125$ kpc), but $z_{gal} = 0.00943$.) Nevertheless, the spectroscopic redshift of SDSS J121838.62+064230.1, $z_{gal} = 0.00669$, is in even better agreement with the absorber redshift than SDSS J121920.67+064218.4. These galaxies are both shown in Figure 12.

Other galaxy–absorber pairs reported along this sightline are:

1. $z_{abs} = 0.0784$–0.0805 and SDSS J121930.87+064334.4 (Bowen et al. 1996; Stocke et al. 2013): This galaxy is excluded from our SDSS galaxy catalog, due to the photometric redshift error cut.
2. $z_{abs} = 0.1240$ and SDSS J121923.43+063819.7 (Mathes et al. 2014): This absorption system consists of 13 components, showing multicomponent Lyα, O VI, C IV, and Si III. This galaxy, with $(z_{phot}, \rho) = (0.1318, 94$ kpc), is the sixth-highest overall probability match to this absorber in the virial radius method, but it is the top match for the stellar mass method. After uniqueness

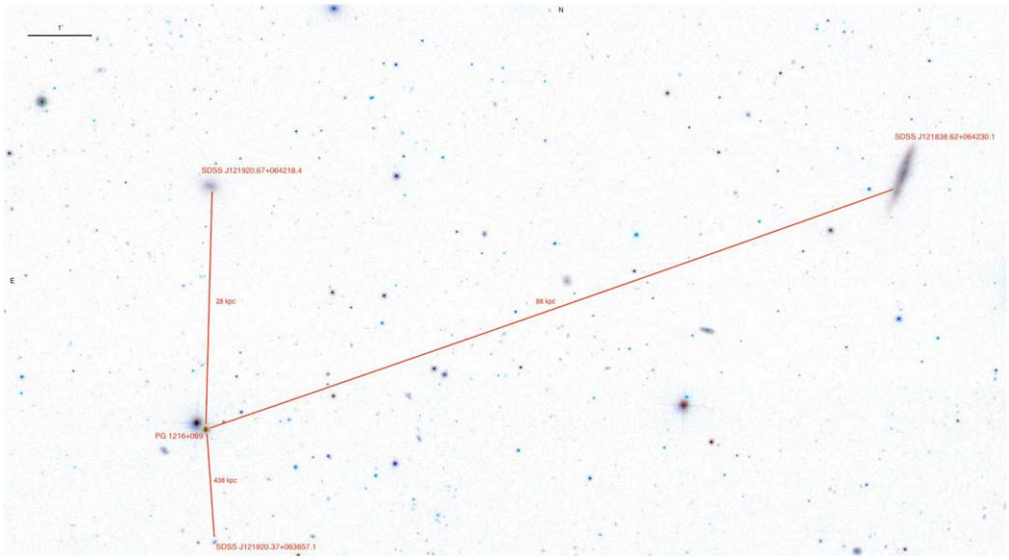

Figure 12. Galaxies SDSS J121920.67+064218.4, (z_{phot}, ρ) = (0.03, 28 kpc) and SDSS J121838.62+064230.1, (z_{phot}, ρ) = (0.019, 88 kpc), paired with $z_{abs} = 0.006$, and SDSS J121920.37+063657.1, (z_{phot}, ρ) = (0.30, 438 kpc) paired with $z_{abs} = 0.282$ in the spectrum of PG 1216+069.

criteria are applied, however, it is the galaxy reported for virial radius method in Table 4. The galaxy's spectroscopic redshift is reported by Keeney et al. (2018) to be $z_{gal} = 0.12365$, and these authors flag it as the closest galaxy to this absorber.

Our two methods identify 14 other possible galaxy–absorber pairs along this rich sightline. One of particular interest is a $z_{abs} = 0.282$ system with Lyα, O VI, Si III, and C III components and SDSS J121920.37+063657.1, (z_{phot}, ρ) = (0.30, 438 kpc), a unique match reported in Table 4. This system is also shown in Figure 12. The stellar mass method uniquely pairs this galaxy with a $z_{abs} = 0.267$ Lyα absorber. This galaxy is not in the spectroscopic sample of Keeney et al. (2018).

A.24. PG 1222+216

Our methods find possible galaxy matches to several multicomponent systems:

1. $z_{abs} = 0.0544$: This absorber shows Si III, Si IV, and C IV in addition to Lyα. Both methods pair it with SDSS J122445.32+212401.1, with (z_{phot}, ρ) = (0.064, 158 kpc). The galaxy is not in the spectroscopic sample of Keeney et al. (2018).
2. $z_{abs} = 0.0987$: This Si IV, C IV, and Lyα system is matched with SDSS J122456.68+212312.2, (z_{phot}, ρ) = (0.091, 74 kpc). Keeney et al. (2018) report a spectroscopic redshift in good agreement with z_{phot} for this galaxy, and it is flagged as the closest to this absorber. This pair is shown in Figure 13.
3. $z_{abs} = 0.222$: This system shows both C III and O VI along with two Lyα components. Both methods choose SDSS J122457.88+212426.1 as the most likely galaxy responsible for this absorber, with (z_{phot}, ρ) = (0.235, 400 kpc). This galaxy is not in the spectroscopic sample of Keeney et al. (2018).
4. $z_{abs} = 0.3773$: This Lyα redshift is one of six in this absorbing complex, along with five O VI components, four C III, and one Si III. Both methods pair this with SDSS J122454.53+212218.3, (z_{phot}, ρ) = (0.394, 147 kpc). This galaxy is not in the spectroscopic sample of Keeney et al. (2018).
5. $z_{abs} = 0.4213$: This system consists of three Lyα lines, two C III, a Si II, two Si III, and an O VI component. It is paired with SDSS J122451.79+212157.6 by (z_{phot}, ρ) = (0.41, 342 kpc) by the virial radius method and with SDSS J122452.68+212337.1, (z_{phot}, ρ) = (0.39, 316 kpc) by the stellar mass method, after uniqueness is imposed.
6. $z_{abs} = 0.4231$: This system of Lyα, C III, and O VI components is matched with SDSS J122455.68+212346.0, (z_{phot}, ρ) = (0.43, 348 kpc), also not part of the spectroscopic sample of Keeney et al. (2018). This pair is also shown in Figure 13.

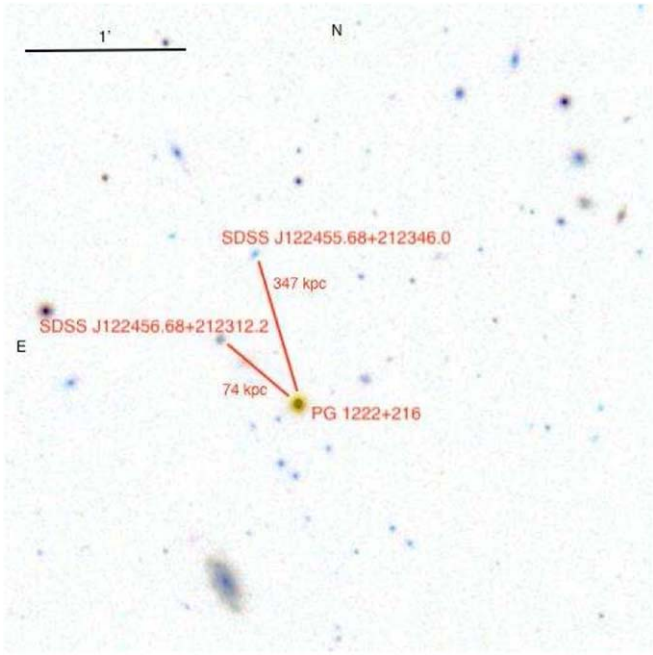

Figure 13. Galaxies SDSS J122456.68+212312.2, (z_{phot}, ρ) = (0.091, 74 kpc) and SDSS J122455.68+212346.0, (z_{phot}, ρ) = (0.43, 348 kpc) paired with $z_{abs} = 0.0987$, 0.423, respectively, in the spectrum of PG 1222+216.

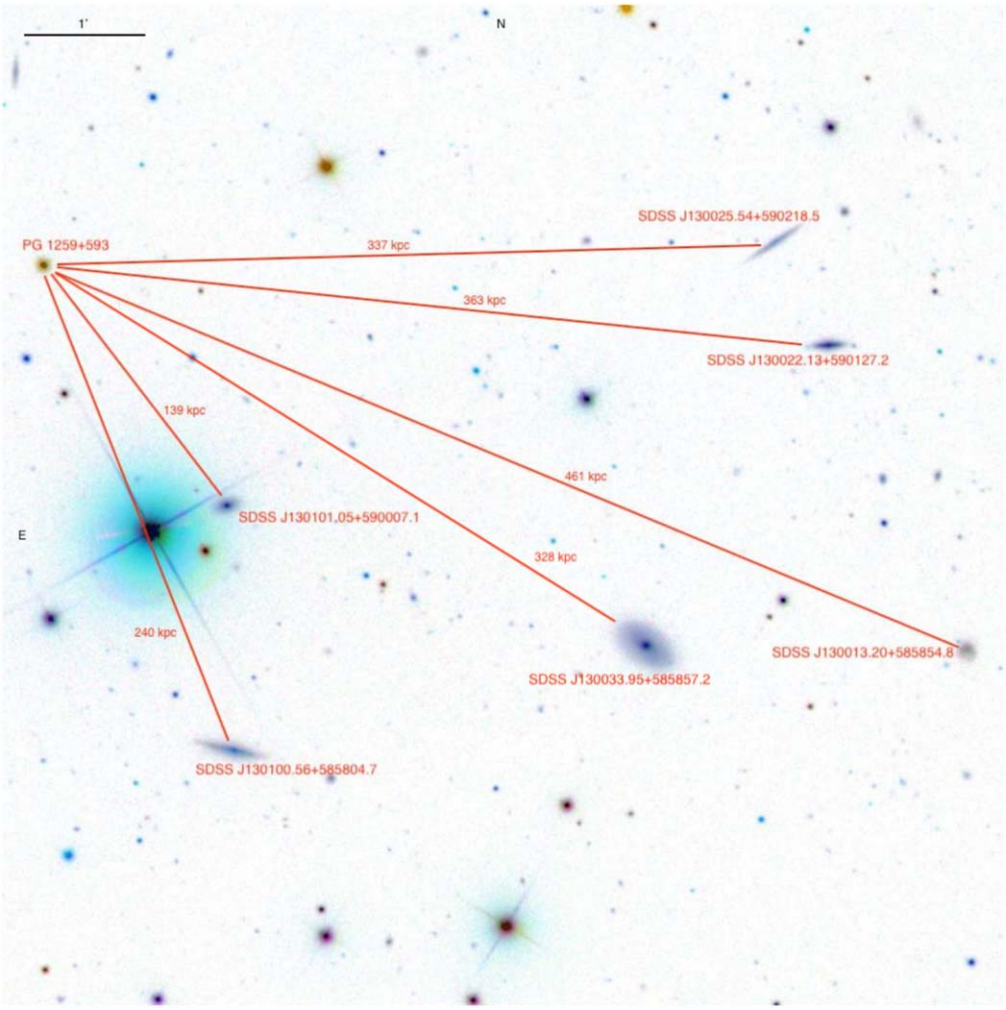

Figure 14. Galaxies SDSS J130101.05+590007.1, (z_{phot}, z_{gal}, ρ) = (0.043, 0.0462, 139 kpc); SDSS J130100.56+585804.7, (z_{phot}, z_{gal}, ρ) = (0.042, 0.0459, 240 kpc); SDSS J130033.95+585857.2, (z_{phot}, z_{gal}, ρ) = (0.033, 0.460, 328 kpc) SDSS J130022.13+590127.2, (z_{phot}, z_{gal}, ρ) = (0.053, 0.0464, 363 kpc); SDSS J130013.20 +585854.8, (z_{phot}, z_{gal}, ρ) = (0.046, 0.04639, 461 kpc); and SDSS J130025.54+590218.5, (z_{phot}, z_{gal}, ρ) = (0.069, 0.04658, 337 kpc), paired with $z_{abs} = 0.046$ in the spectrum of PG 1259+593.

A.25. PG 1229+204

Côté et al. (2005) associate UGC 7697 with $z_{abs} = 0.00859$, but this galaxy is excluded from our galaxy sample, due to the photometric redshift error cut. We find five other potential galaxy–absorber pairs, all with $\rho > 300$ kpc.

A.26. PG 1259+593

This sightline has been studied by several authors, finding the following galaxy–absorber pairs:

1. $z_{abs} = 0.00229$: Côté et al. (2005) associate this absorber with UGC 8146, while Stocke et al. (2013) report another possible associated galaxy, SDSS J130207.44+584153.8. Both galaxies are excluded from our catalog, due to the photometric redshift error cut we employ.
2. $z_{abs} = 0.00759$: Wakker & Savage (2009) pair this absorber with UGC 8040. This galaxy is the fifth-best match to the absorber in both methods, in part due to its photometric redshift, $z_{phot} = 0.019$. The unique galaxy match to the absorber found by both methods is SDSS J125503.96+584728.8, with (z_{phot}, ρ) = (0.012, 472 kpc). The spectroscopic redshift of this galaxy, $z_{gal} = 0.00874$, places it within ~350 km s^{-1} of this $z_{abs} = 0.00759$ absorber.
3. $z_{abs} = 0.046$: This absorber shows Lyα, Si II, Si III, and C IV components. Stocke et al. (2013) discuss the association of two absorbers, with $z_{abs} = 0.0460$ and $z_{abs} = 0.0464$ with SDSS J130101.05+590007.1, $z_{gal} = 0.0462$, and with other members of a possible galaxy group, including SDSS J130033.95+585857.2 ($z_{gal} = 0.0460$), SDSS J130100.56+585804.7 ($z_{gal} = 0.0459$), and SDSS J130022.13+590127.2 ($z_{gal} = 0.0464$). The galaxy with the highest overall probabilities for both methods is SDSS J130101.05+590007.1, but due to the emphasis the uniqueness algorithm places on the Lyα P_{ion}, the unique pairing listed in Tables 4 and 5 is the second-highest probability match, SDSS J130100.56+585804.7, (z_{phot}, ρ) = (0.042, 240 kpc). Its SDSS spectrum shows it to be a star-forming galaxy. Other possible group galaxies found in the top 10 probable galaxies paired with this absorber by the virial radius method are: SDSS J130033.95+585857.2, with (z_{phot}, ρ) = (0.033, 328 kpc); SDSS J130022.13 +590127.2, with (z_{phot}, ρ) = (0.053, 363 kpc); SDSS J130013.20+585854.8, a star-forming galaxy with $z_{gal} = 0.04639$; and SDSS J130025.54+590218.5

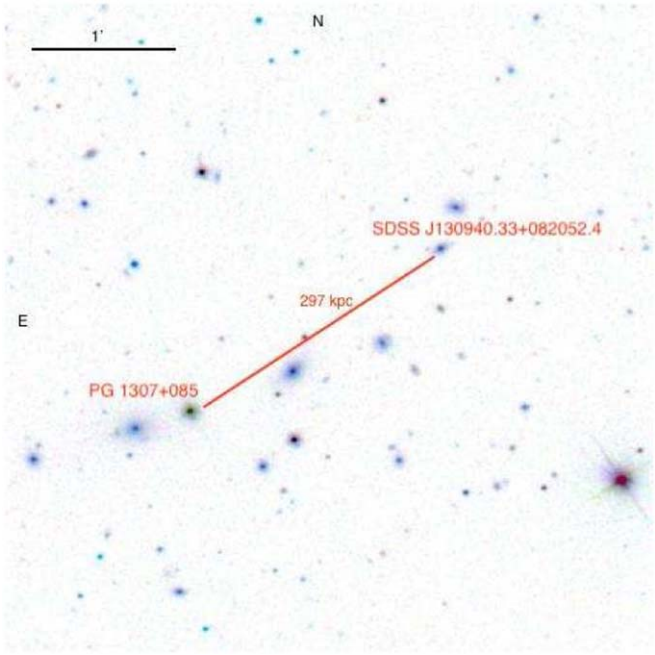

Figure 15. Galaxy SDSS J130940.33+082052.4, (z_{phot}, ρ) = (0.145, 297 kpc) paired with $z_{abs} = 0.14$ in the spectrum of PG 1307+085.

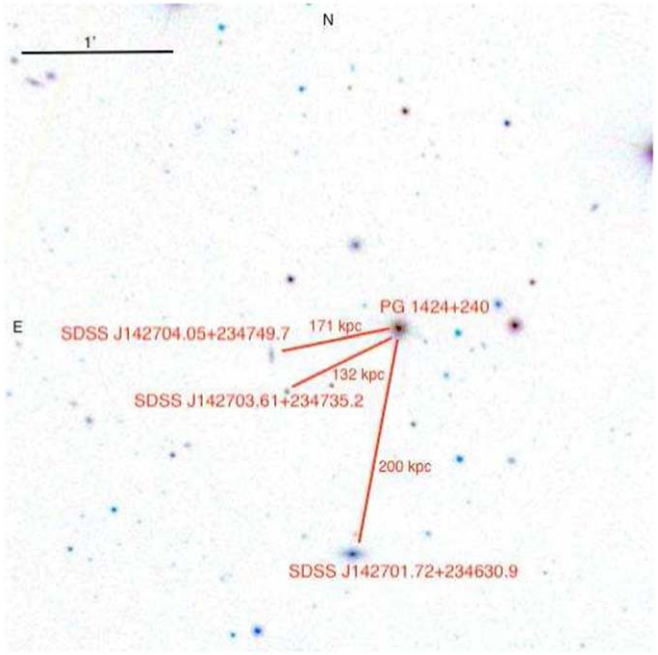

Figure 16. Galaxies SDSS J142701.72+234630.9, (z_{phot}, ρ) = (0.12, 200 kpc); SDSS J142703.61+234735.2, (z_{phot}, ρ) = (0.15, 132 kpc); and SDSS J142704.05+234749.7, (z_{phot}, ρ) = (0.19, 171 kpc), paired with absorbers in the spectrum of PG 1424+240.

($z_{gal} = 0.04658$). All of these galaxies are shown in Figure 14.

4. $z_{abs} = 0.196$: Mathes et al. (2014) associate this absorber with SDSS J130116.43+590135.7, which is only the seventh (eighth) best match with the virial radius (stellar mass) method, due to its photometric redshift estimate, $z_{phot} = 0.3517$. After imposing the uniqueness criteria, the galaxy matched with this absorber in Tables 4 or 5 is the second-most probable match, SDSS J130131.84+590128.5, (z_{phot}, ρ) = (0.26, 495 kpc). However, Keeney et al. (2018) report $z_{gal} = 0.24076$, which is in better agreement with the absorber discussed below.
5. $z_{abs} = 0.241$: Mathes et al. (2014) find that this absorber is associated with SDSS J130109.88+590315.3, the fifth-best match found by our two methods. Instead, our methods give a top match with SDSS J130059.79+590059.7, (z_{phot}, ρ) = (0.36, 466 kpc). This galaxy is uniquely paired with $z_{abs} = 0.256$ in Tables 4 and 5. Keeney et al. (2018) report the spectroscopic redshift of SDSS J130059.79+590059.7 to be 0.2929, so it is unlikely to be truly associated with either of these absorbers, but instead with $z_{abs} = 0.292$.

One remaining absorption system along this line of sight is a $z_{abs} = 0.22$ system showing Lyα, O VI, Si III, and C III. We do find a galaxy paired with this absorber, SDSS J130059.79+590059.7, (z_{phot}, ρ) = (0.35, 435 kpc), but its association with the absorber would depend on its true redshift being substantially different from the photometric estimate. There is no spectroscopic redshift reported by Keeney et al. (2018).

A.27. PG 1307+085

This sightline has no reported galaxy–absorber pairs reported in the literature. There are only four possible unique pairs meeting the probability threshold reported by both methods in Tables 4 and 5, including a multicomponent $z_{abs} = 0.14$ system with Lyα and O VI matched with SDSS J130940.33+082052.4, with (z_{phot}, ρ) = (0.145, 297 kpc). This is shown in Figure 15.

A.28. PG 1309+355

Côté et al. (2005) associate $z_{abs} = 0.00292$ absorber with the NGC 5033 group. We report seven (nine) potential galaxy–absorber pairs meeting the 10% probability threshold found using the virial radius (stellar mass) method, including one galaxy, SDSS J131220.99+351518.3 (($z_{phot} = 0.15$), paired with $z_{abs} = 0.0877$ ($\rho = 65$ kpc) by the virial radius method and $z_{abs} = 0.120$ ($\rho = 87$ kpc) by the stellar mass method.

A.29. PG 1424+240

We find 24 possible galaxy–absorber pairs for this sightline, including:

1. $z_{abs} = 0.12$: This system showing Lyα, O VI, Si III, and C IV) and SDSS J142701.72+234630.9, (z_{phot}, ρ) = (0.12, 200 kpc), in agreement with the spectroscopic measurement $z_{gal} = 0.1211$. This pair is shown in Figure 16.
2. $z_{abs} = 0.14$: This system with Lyα, O VI, Si III, Si IV, and C IV, is paired as a unique match with SDSS J142703.61+234735.2, (z_{phot}, ρ) = (0.15, 132 kpc), which is shown in Figure 16. This galaxy is not in the sample of Keeney et al. (2018), who report the closest galaxy to this absorber having an impact parameter of 493 kpc.
3. $z_{abs} = 0.20$: This absorber with one Lyα and two C III components is paired with SDSS J142704.05+234749.7, (z_{phot}, ρ) = (0.20, 171 kpc) by the virial radius method. This pair is shown in Figure 16, and is marginally favored over the pairing reported by the stellar mass method, SDSS J142701.63+234833.0, (z_{phot}, ρ) = (0.19, 124 kpc). Neither galaxy is part of the spectroscopic sample of

Keeney et al. (2018), who report the closest galaxy to this absorber having an impact parameter of 683 kpc.

A.30. PG 1626+554

Our methods find eight potential galaxies paired with single Lyα lines along this line of sight. All but one have $\rho \sim 400$–500 kpc. One pair, $z_{abs} = 0.0613$ and SDSS J162828.16+552648.4, $(z_{phot}, \rho) = (0.060, 446$ kpc), is supported by the spectroscopic redshift measurement reported by Keeney et al. (2018), $z_{gal} = 0.06168$.

A.31. PG 2349+014

Bowen et al. (1997) find an association between a $z_{abs} = 0.038$ system showing Lyα and Si III in the COS spectrum and SDSS J235142.21-010100.9. This is recovered as the most favored galaxy matched to this absorber by both methods $(z_{phot}, \rho) = (0.043, 406$ kpc), and reported as the unique match for the virial radius method. But our uniqueness criteria with the stellar mass method instead pair this galaxy with a $z_{abs} = 0.0455$ Lyα line. We find 8(9) other possible galaxy– Lyα absorber pairs with the virial radius (stellar mass) method.

A.32. QSO 0045+3926

This sightline has no reported galaxy–absorber pairs reported in the literature. We find six (seven) possible pairs with the virial radius(stellar mass) method, including a $z_{abs} = 0.110$ Lyα and O VI system associated with SDSS J004833.42+394057.1, $(z_{phot}, \rho) = (0.12, 339$ kpc).

A.33. Q 1230+0115

As for 3C 273 and PG 1216+069, the Virgo cluster lies in the foreground. Penton et al. (2002) and Wakker & Savage (2009) note a correspondence between $z_{abs} = 0.00769$ and UGC 7625. The SDSS photometric redshift estimate for this galaxy is 0.114, so it is not in the top 10 most probable matches we find for this absorber. Our algorithms identify SDSS J122815.96+014944.1, $(z_{phot}, \rho) = (0.013, 495$ kpc), as the unique galaxy match for this absorber. However, the spectroscopic redshift reported by SDSS, $z_{gal} = 0.0030$, contradicts this result.

Our highest-probability unique match from the virial radius method to a $z_{abs} = 0.0057$ system with five Lyα, two C II, one Si II, one Si III, and two Si IV components is SDSS J122921.63+010325.0, $(z_{phot}, \rho) = (0.018, 194$ kpc). However, the spectroscopic redshift, $z_{gal} = 0.0231$, does not support an association.

A more promising association found by the stellar mass method between a $z_{abs} = 0.031$ Lyα and C IV system and SDSS J123034.42+011624.4, with $(z_{phot}, \rho) = (0.031, 151$ kpc). The spectroscopic redshift is in good agreement in this case, $z_{gal} = 0.031$, and this pair is shown in Figure 17. The unique galaxy match to the absorber found by the virial radius method, SDSS J123141.38+011821.5, $(z_{phot}, \rho) = (0.048, 495$ kpc), is less plausible, both because of the large impact parameter and because SDSS reports $z_{gal} = 0.0234$.

Finally, our methods both find a match of a $z_{abs} = 0.077$ C IV, Si IV, and Si III system with SDSS J123047.60+011518.6, $(z_{phot}, \rho) = (0.12, 53$ kpc). This is supported by the spectroscopic redshift reported by Keeney et al. (2018), $z_{gal} = 0.07782$, and is also shown in Figure 17.

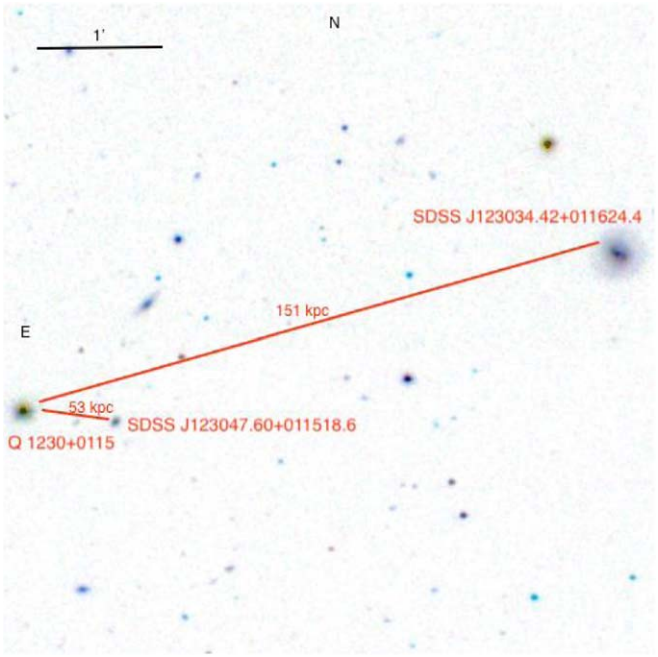

Figure 17. Galaxy SDSS J123034.42+011624.4, $(z_{phot}, \rho) = (0.031, 151$ kpc), paired with $z_{abs} = 0.031$, and galaxy SDSS J123047.60+011518.6, $(z_{phot}, \rho) = (0.12, 53$ kpc), paired with $z_{abs} = 0.077$, in the spectrum of Q 1230+0115.

A.34. SBS 1108+560

Stocke et al. (2013) find an association of M 108 with two possible absorbers, $z_{abs} = 0.0222$ and $z_{abs} = 0.0259$. This galaxy is excluded from our SDSS galaxy sample due to its brightness and large projected size on the sky. Liang & Chen (2014) report that the galaxy WISEA J111125.60+554435.4 is a pair with $z_{abs} = 0.138$. This galaxy is our top match to the absorber with both methods. However, after imposing the uniqueness criteria on the stellar mass method results, the unique galaxy paired with this absorber and reported in Table 5 is SDSS J111116.84+554812.2 $(z_{phot}, \rho) = (0.142, 339$ kpc), and Keeney et al. (2018) report its spectroscopic redshift to be $z_{gal} = 0.13813$, an even better redshift match with z_{abs}.

Between the two methods, we report 22 other possible galaxy–absorber pairs for this sightline. One possible pair identified by both methods is $z_{abs} = 0.0548$ and SDSS J111141.44+554424.3, $(z_{phot}, \rho) = (0.057, 212$ kpc). The spectroscopic redshift reported by Keeney et al. (2018), $z_{gal} = 0.05493$, supports this association, and the pair is shown in Figure 18. These authors report that another SDSS galaxy lies closer than SDSS J111141.44+554424.3 to the absorber.

The candidate pairs also include a $z_{abs} = 0.33$ O VI absorber, uniquely paired with SDSS J111132.78+554817.9, $(z_{phot}, \rho) = (0.33, 253$ kpc) by the virial radius method. This galaxy is the top stellar mass method match to the absorber also, but the uniqueness criteria match it with two $z_{abs} = 0.285$ Lyα absorbers, and no unique match is listed for $z_{abs} = 0.33$. This pair is shown in Figure 18.

The stellar mass method yields a match of a $z_{abs} = 0.46$ system with O VI, Si III, and C III and SDSS J111132.33+554712.8, $(z_{phot}, \rho) = (0.43, 78$ kpc). The galaxy's spectroscopic redshift, $z_{gal} = 0.462$, supports this association. This pair is also shown in Figure 18. The virial radius method finds this galaxy as the top match to the $z_{abs} = 0.46$ system also, but the uniqueness criteria match it with an O VI—only $z_{abs} = 0.4358$ absorber.

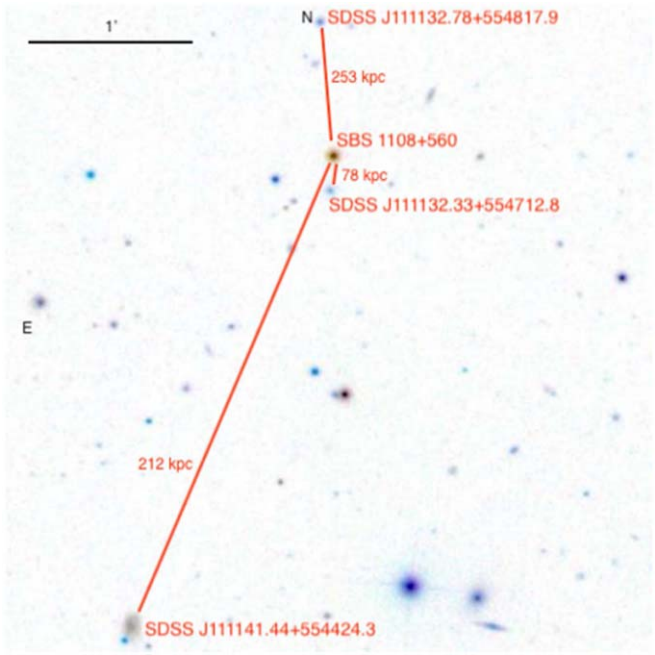

Figure 18. Galaxies SDSS J111141.44+554424.3, ($z_{\rm phot}$, ρ) = (0.057, 212 kpc), SDSS J111132.78+554817.9, ($z_{\rm phot}$, ρ) = (0.33, 253 kpc), and SDSS J111132.33+554712.8, ($z_{\rm phot}$, ρ) = (0.43, 78 kpc), paired with $z_{\rm abs} = 0.140$, 0.32, 0.46, respectively, in the spectrum of SBS 1108+560.

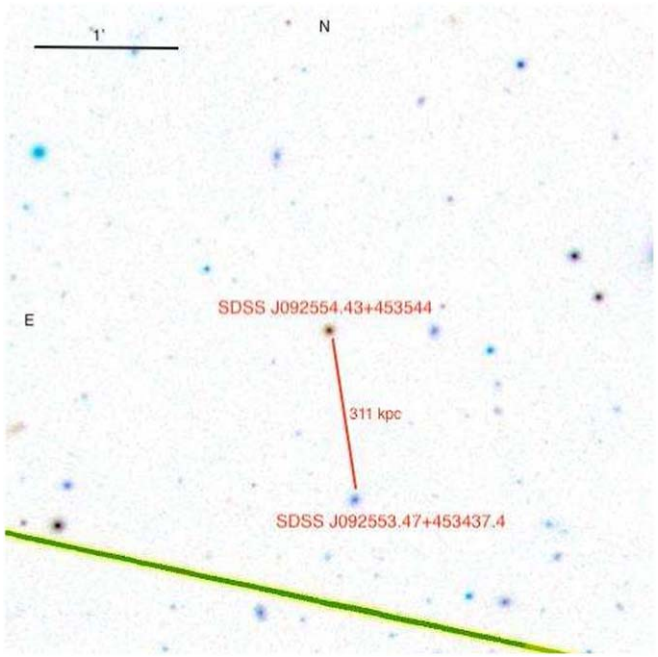

Figure 19. Galaxy SDSS J092553.47+453437.4, ($z_{\rm phot}$, ρ) = (0.30, 311 kpc) paired with $z_{\rm abs} = 0.309$ absorber in the spectrum of QSO SDSS J080908.13+461925.6.

A.35. SBS 1122+594

In total, our virial radius (stellar mass) method identifies 28 (27) possible galaxy–absorber pairs for this long line of sight to the $z = 0.852$ QSO. Stocke et al. (2013) and Liang & Chen (2014) determine an association between $z_{\rm abs} = 0.04$ and IC 691. This galaxy is excluded from our SDSS galaxy lists because of our photometric redshift error cut. Instead, our methods find SDSS J112505.99+591804.6 as the reported match for this Lyα line, with ($z_{\rm phot}$, ρ) = (0.06, 477 kpc). The spectroscopic redshift of this galaxy is 0.1125, so this is not considered a more likely association than IC 691.

Other galaxy–absorber pairs found along this sightline include:

1. $z_{\rm abs} = 0.060$: This system shows Lyα, C IV, Si IV, and Si III absorption. The virial radius method finds a match with SDSS J112517.67+590828.8, ($z_{\rm phot}$, ρ) = (0.064, 350 kpc). The SDSS spectroscopic redshift is $z_{\rm gal} = 0.058$, a difference of $\sim$565 km s^{-1} with the absorber redshift.
2. $z_{\rm abs} = 0.138$: This system consists of four Lyα lines. Both methods yield a match with SDSS J112618.11+590925.8, ($z_{\rm phot}$, ρ) = (0.13, 481 kpc). This galaxy is not part of the Keeney et al. (2018) sample.
3. $z_{\rm abs} = 0.194$: For this system showing O VI, Si III, and C III absorption, both methods uniquely pair SDSS J112549.24+590957.7, ($z_{\rm phot}$, ρ) = (0.18, 137 kpc). However, given the spectroscopic redshift reported by Keeney et al. (2018), $z_{\rm gal} = 0.15527$, this galaxy is more likely associated with $z_{\rm abs} = 0.155$, as these authors note it is the closest galaxy known.
4. $z_{\rm abs} = 0.420$: This O VI system is matched with SDSS J112548.53+590916.8, ($z_{\rm phot}$, ρ) = (0.40, 426 kpc). This galaxy is not in the spectroscopic sample of Keeney et al. (2018).

A.36. SDSS J080908.13+461925.6

For this sightline, we find 18 (16) possible galaxy–absorber pairs with the virial radius (stellar mass) method. Liang & Chen (2014) report that the $z_{\rm abs} = 0.0464$ system, with Lyα, Si III, and Si IV, is associated with SDSS J080913.17+461842.7. This is the top match for the virial radius method, and the second-most probable match for the stellar mass method. The other top match for both methods is SDSS J080914.28+461822.2, ($z_{\rm phot}$, ρ) = (0.044, 82 kpc), which is reported as the unique pairing in Tables 4 and 5.

A.37. SDSS J092554.43+453544

We find 25 possible galaxy–absorber pairs with both methods. Liang & Chen (2014) report two galaxy–absorber pairs for this sightline: $z_{\rm abs} = 0.0170$ and SDSS J092721.06+454158.8, the second match to the absorber and the unique pair outcome of both our methods; and $z_{\rm abs} = 0.0261$ and SDSS J092617.38+452924.9, the top match from the virial radius method and the second match to the absorber from the stellar mass method. For $z_{\rm abs} = 0.0261$, the unique galaxy match is instead with the second virial radius method match and the top stellar mass method match, SDSS J092530.98+453157.8, ($z_{\rm phot}$, ρ) = (0.027, 183 kpc). However, the SDSS spectroscopic redshift of this galaxy is 0.0142, which does not support this proposed association.

Our methods also match a $z_{\rm abs} = 0.296$ system with O VI and C III absorption with SDSS J092556.40+453653.3, ($z_{\rm phot}$, ρ) = (0.28, 320 kpc); and a $z_{\rm abs} = 0.309$ system with O VI and C III with SDSS J092553.47+453437.4, ($z_{\rm phot}$, ρ) = (0.30, 311 kpc), shown in Figure 19. The spectroscopic redshift of SDSS J092553.47+453437.4, $z_{\rm gal} = 0.3088$, does support this association.

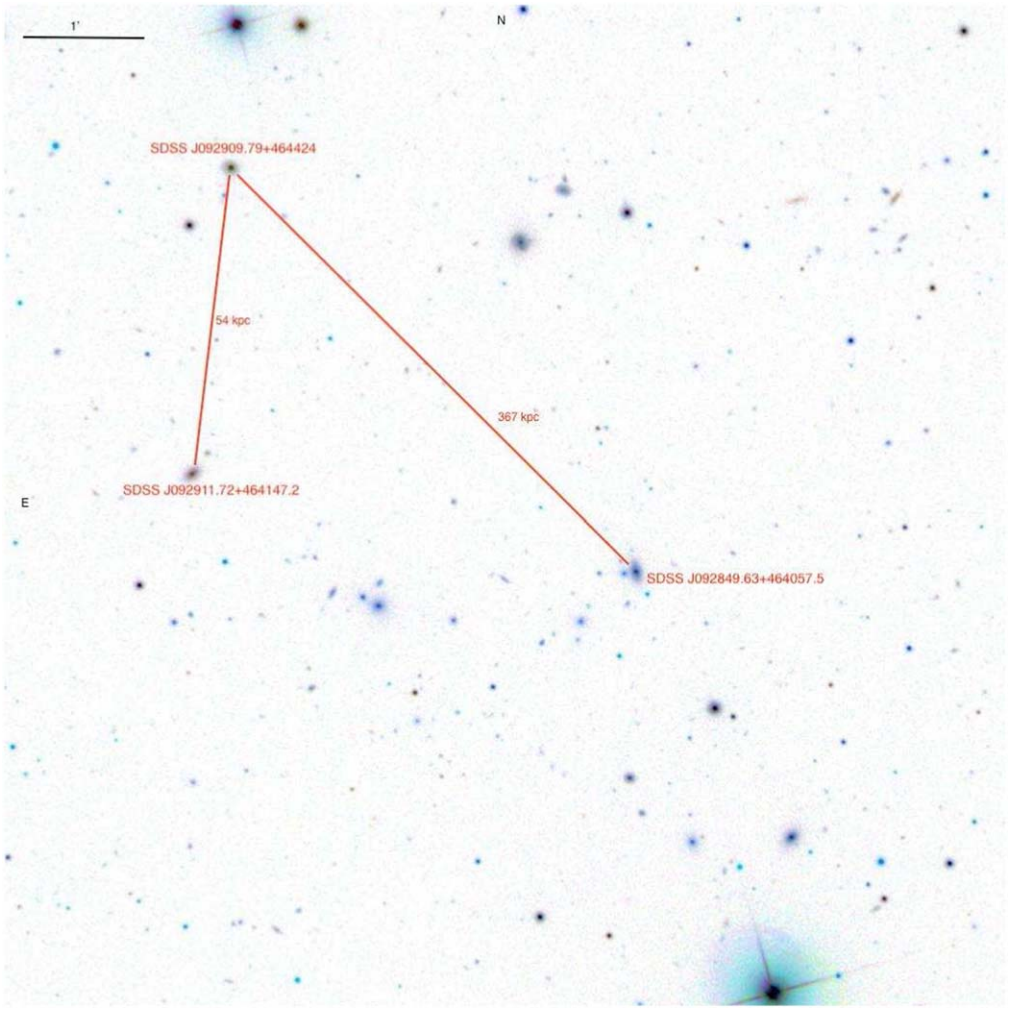

Figure 20. Galaxies SDSS J092911.72+464147.2, ($z_{\rm phot}$, ρ) = (0.012, 54 kpc) and SDSS J092849.63+464057.5, ($z_{\rm phot}$, ρ) = (0.065, 367 kpc), paired with absorbers in the spectrum of QSO SDSS J092909.79+464424.

A.38. SDSS J092909.79+464424

With both methods, we find 18 potential galaxy absorber pairs. Some candidates of particular interest include:

1. $z_{\rm abs} = 0.016$: a C IV system matched with SDSS J092911.72+464147.2, ($z_{\rm phot}$, ρ) = (0.012, 54 kpc) and spectroscopic redshift $z_{\rm gal} = 0.01676$. This pair is shown in Figure 20.
2. $z_{\rm abs} = 0.064$: a double Lyα component system paired with SDSS J092849.63+464057.5, ($z_{\rm phot}$, ρ) = (0.065, 367 kpc) and spectroscopic redshift $z_{\rm gal} = 0.06402$. This pair is shown in Figure 20.
3. $z_{\rm abs} = 0.145$: an O VI absorber and SDSS J092853.27+464412.6 by ($z_{\rm phot}$, ρ) = (0.10, 435 kpc).

A.39. SDSS J094952.91+390203

We find 14 galaxy–absorber pairs for this sightline with both methods. Liang & Chen (2014) report a pairing of $z_{\rm abs} = 0.0669$ with SDSS J095002.76+390308.7. This is our top-ranked galaxy match to this absorber, with ($z_{\rm phot}$, ρ) = (0.058, 159 kpc).

We also find a $z_{\rm abs} = 0.018$ system showing Lyα, Si III, and C IV components with SDSS J094945.57+390101.9, ($z_{\rm phot}$, ρ) = (0.027, 39 kpc), shown in Figure 21. The spectroscopic redshift of the galaxy, $z_{\rm gal} = 0.0180$, is in excellent agreement with $z_{\rm abs}$. Finally, we report the match of a $z_{\rm abs} = 0.164$ double Lyα component system with SDSS J094953.16+385914.6, ($z_{\rm phot}$, ρ) = (0.164, 480 kpc). This pair is also shown in Figure 21.

A.40. SDSS J135712.61+170444

We report seven possible galaxy–absorber pairs for this QSO sightline. One is a rich metal line system: a $z_{\rm abs} = 0.097$ system with Si III, Si IV, C II, and C IV paired with SDSS J135719.68+170410.3, ($z_{\rm phot}$, ρ) = (0.10, 195 kpc). However, the galaxy's SDSS spectroscopic redshift, $z_{\rm gal} = 0.12605$, does not support this pairing.

On the other hand, a $z_{\rm abs} = 0.083$ system that shows absorption from multiple components of Si III, Si IV, and C IV is matched with SDSS J135716.36+170430.4, ($z_{\rm phot}$, ρ) = (0.087, 88 kpc). Its spectroscopic redshift, $z_{\rm gal} = 0.08334$, does support the association. This pair is shown in Figure 22.

A.41. TON 1187

We find eight candidate galaxy–absorber pairs for this line of sight with the two methods, all consisting of Lyα only. One absorber, $z_{\rm abs} = 0.0678$, is paired with a galaxy with $\rho = 117$ kpc, SDSS J101255.81+355120.4. A true association

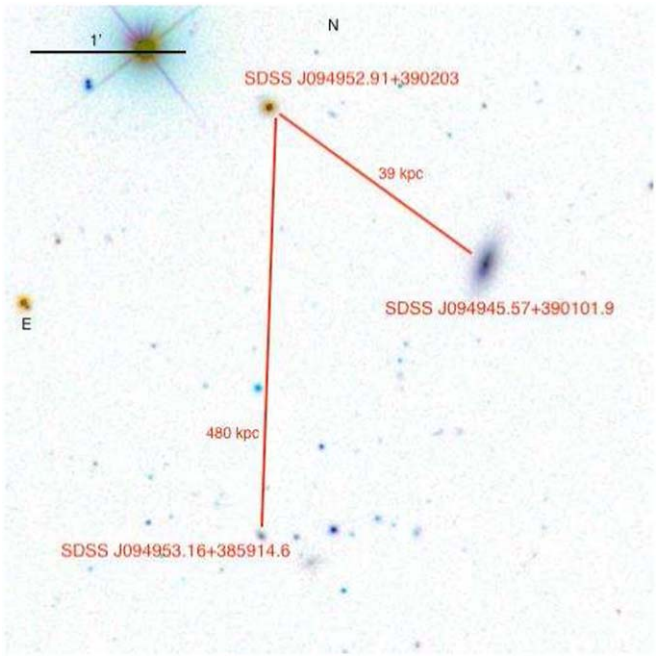

Figure 21. Galaxies SDSS J094945.57+390101.9, ($z_{\rm phot}$, ρ) = (0.027, 39 kpc) and SDSS J094953.16+385914.6, ($z_{\rm phot}$, ρ) = (0.164, 480 kpc), paired with absorbers in the spectrum of QSO SDSS J094952.91+390203.

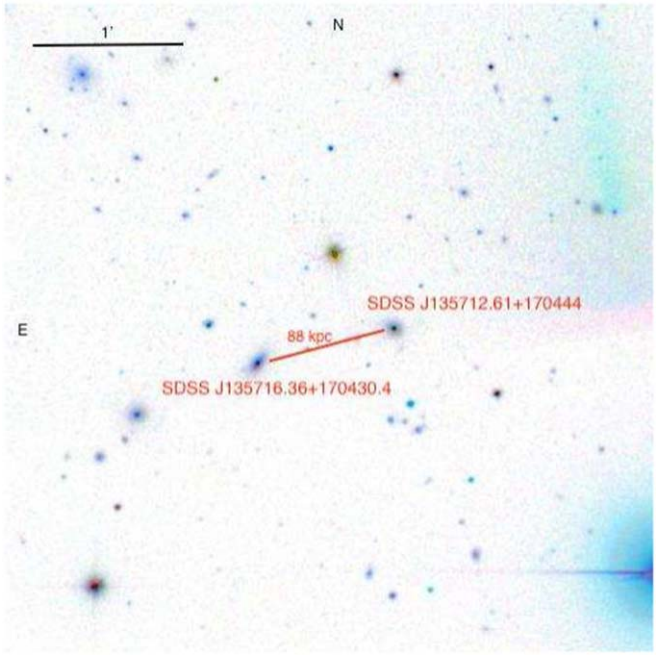

Figure 22. Galaxy SDSS J135716.36+170430.4, ($z_{\rm phot}$, ρ) = (0.087, 88 kpc), paired with $z_{\rm abs} = 0.083$ absorber in the spectrum of QSO SDSS J135712.61 +170444.

depends on a better redshift agreement between $z_{\rm abs}$ and the spectroscopic redshift than with the photometric estimate, $z_{\rm phot} = 0.076$.

Another pair, a three-component $z_{\rm abs} = 0.035$ system and SDSS J101222.19+355523.0, ($z_{\rm phot}$, ρ) = (0.039, 394 kpc), is unlikely, given the fact that $z_{\rm gal} = 0.0393$. Instead, this galaxy is likely a better match with $z_{\rm abs} = 0.04022$ ($\rho = 443$ kpc), for which it is the top-ranked pairing before the uniqueness criteria are imposed.

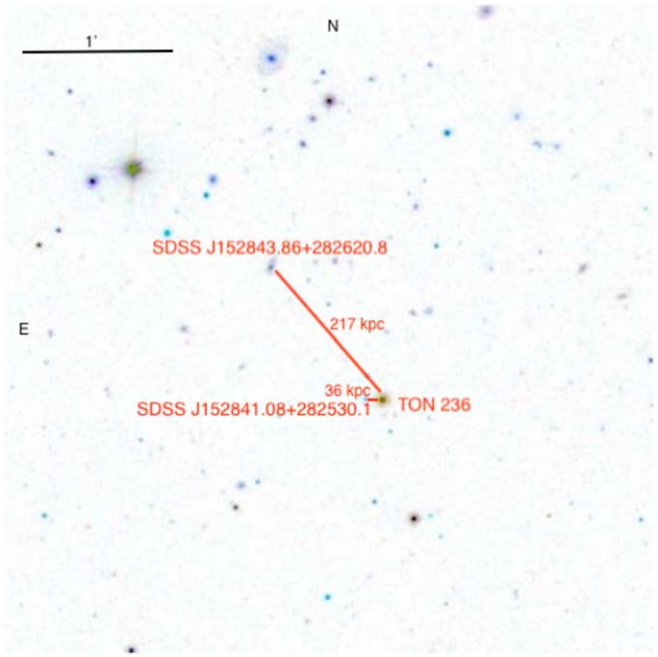

Figure 23. Galaxies SDSS J152843.86+282620.8, ($z_{\rm phot}$, ρ) = (0.14, 217 kpc) and SDSS J152841.08+282530.1, ($z_{\rm phot}$, ρ) = (0.47, 36 kpc), paired with absorbers in the spectrum of TON 236.

A.42. TON 236

Liang & Chen (2014) report an association of with $z_{\rm abs} = 0.0451$ with SDSS J152827.39+282738.6. This galaxy is excluded from our SDSS galaxy catalog due to the photometric redshift error cut we employ.

Our methods yield 20 possible galaxy–absorber pairs for this QSO sightline. An O VI system with $z_{\rm abs} = 0.194$ is matched with SDSS J152843.86+282620.8, ($z_{\rm phot}$, ρ) = (0.14, 217 kpc) with both methods. This galaxy has no measured spectroscopic redshift. The pair is shown in Figure 23.

A $z_{\rm abs} = 0.259$ O VI absorber is paired with SDSS J152845.56+282654.6, ($z_{\rm phot}$, ρ) = (0.25, 434 kpc) by both methods. This galaxy is not in the Keeney et al. (2018) sample.

Finally, we note that our methods each pair a galaxy very close to the sightline, SDSS J152841.08+282530.1, with two different absorption systems, as defined by our algorithm. The virial radius method pairs the galaxy with a triple-component $z_{\rm abs} = 0.433$ Lyα absorber, and the stellar mass method pairs it with a double-component $z_{\rm abs} = 0.439$ Lyα absorber. This galaxy is also not in the spectroscopic sample of Keeney et al. (2018). It is shown in Figure 23.

A.43. TON 580

Liang & Chen (2014) find that a $z_{\rm abs} = 0.0744$ C IV system is associated with SDSS J113056.11+311445.6 at $\rho = 250$ kpc. We recover this pairing as the top match with both of our methods. We report 14 other galaxy–Lyα absorber pairs for this sightline. One match, $z_{\rm abs} = 0.1023$ paired with SDSS J113121.67+311055.8, ($z_{\rm phot}$, ρ) = (0.125, 464 kpc), is ruled out by the spectroscopic redshift reported by Keeney et al. (2018), $z_{\rm gal} = 0.12434$. A $z_{\rm abs} = 0.2026$ metal system with O VI, C III, and Si III components is matched with SDSS J113108.50+311332.6, ($z_{\rm phot}$, ρ) = (0.224, 116 kpc).

ORCID iDs

Jennifer E. Scott https://orcid.org/0000-0002-8425-3640
Emileigh S. Shoemaker https://orcid.org/0000-0002-4496-9732
Colin D. Hamill https://orcid.org/0000-0002-9464-8494

References

Alam, S., Albareti, F. D., Allende Prieto, C., et al. 2015, ApJS, 219, 12
Bahcall, J. N., & Salpeter, E. E. 1965, ApJ, 142, 1677
Bahcall, J. N., & Spitzer, L. J. 1969, ApJL, 156, L63
Beck, R., Dobos, L., Budavári, T., Szalay, A. S., & Csabai, I. 2016, MNRAS, 460, 1371
Bennett, C. L., Larson, D., Weiland, J. L., & Hinshaw, G. 2014, ApJ, 794, 135
Bielby, R. M., Stott, J. P., Cullen, F., et al. 2019, MNRAS, 486, 21
Bordoloi, R., Prochaska, J. X., Tumlinson, J., et al. 2018, ApJ, 864, 132
Bordoloi, R., Tumlinson, J., Werk, J. K., et al. 2014, ApJ, 796, 136
Borthakur, S., Heckman, T., Strickland, D., Wild, V., & Schiminovich, D. 2013, ApJ, 768, 18
Borthakur, S., Heckman, T., Tumlinson, J., et al. 2015, ApJ, 813, 46
Borthakur, S., Heckman, T., Tumlinson, J., et al. 2016, ApJ, 833, 259
Bowen, D. V., Blades, J. C., & Pettini, M. 1995, ApJ, 448, 634
Bowen, D. V., Blades, J. C., & Pettini, M. 1996, ApJ, 464, 141
Bowen, D. V., Osmer, S. J., Blades, J. C., & Tytler, D. 1997, MNRAS, 284, 599
Bowen, D. V., Pettini, M., & Blades, J. C. 2002, ApJ, 580, 169
Burchett, J. N., Elek, O., Tejos, N., et al. 2020, ApJL, 891, L35
Burchett, J. N., Tripp, T. M., Bordoloi, R., et al. 2016, ApJ, 832, 124
Burchett, J. N., Tripp, T. M., Prochaska, J. X., et al. 2015, ApJ, 815, 91
Chen, H.-W., & Lanzetta, K. M. 2003, ApJ, 597, 706
Chen, H.-W., Lanzetta, K. M., & Webb, J. K. 2001a, ApJ, 556, 158
Chen, H.-W., Lanzetta, K. M., Webb, J. K., & Barcons, X. 1998, ApJ, 498, 77
Chen, H.-W., Lanzetta, K. M., Webb, J. K., & Barcons, X. 2001b, ApJ, 559, 654
Chen, H.-W., & Mulchaey, J. S. 2009, ApJ, 701, 1219
Chen, H.-W., Prochaska, J. X., Weiner, B. J., Mulchaey, J. S., & Williger, G. M. 2005, ApJL, 629, L25
Chilingarian, I. V., Melchior, A.-L., & Zolotukhin, I. Y. 2010, MNRAS, 405, 1409
Chilingarian, I. V., & Zolotukhin, I. Y. 2012, MNRAS, 419, 1727
Côté, S., Wyse, R. F. G., Carignan, C., Freeman, K. C., & Broadhurst, T. 2005, ApJ, 618, 178
Danforth, C. W., Keeney, B. A., Tilton, E. M., et al. 2016, ApJ, 817, 111
Gunn, J. E., & Peterson, B. A. 1965, ApJ, 142, 1633
Heckman, T., Borthakur, S., Wild, V., Schiminovich, D., & Bordoloi, R. 2017, ApJ, 846, 151
Johnson, S. D., Chen, H.-W., & Mulchaey, J. S. 2015, MNRAS, 452, 2553
Johnson, S. D., Chen, H.-W., Mulchaey, J. S., Schaye, J., & Straka, L. A. 2017, ApJL, 850, L10
Keeney, B. A., Stocke, J. T., Danforth, C. W., et al. 2017, ApJS, 230, 6
Keeney, B. A., Stocke, J. T., Pratt, C. T., et al. 2018, ApJS, 237, 11
Lanzetta, K. M., Bowen, D. V., Tytler, D., & Webb, J. K. 1995, ApJ, 442, 538
Liang, C. J., & Chen, H.-W. 2014, MNRAS, 445, 2061
Mathes, N. L., Churchill, C. W., Kacprzak, G. G., et al. 2014, ApJ, 792, 128
McQuinn, M. 2016, ARA&A, 54, 313
Meiksin, A. A. 2009, RvMP, 81, 1405
Morris, S. L., Weymann, R. J., Dressler, A., et al. 1993, ApJ, 419, 524
Muzahid, S. 2014, ApJ, 784, 5
Nelson, D., Pillepich, A., Springel, V., et al. 2019, MNRAS, 490, 3234
Oppenheimer, B. D., Schaye, J., Crain, R. A., Werk, J. K., & Richings, A. J. 2018, MNRAS, 481, 835
Peeples, M. S., Corlies, L., Tumlinson, J., et al. 2019, ApJ, 873, 129
Penton, S. V., Stocke, J. T., & Shull, J. M. 2002, ApJ, 565, 720
Pointon, S. K., Kacprzak, G. G., Nielsen, N. M., et al. 2019, ApJ, 883, 78
Prochaska, J. X., Burchett, J. N., Tripp, T. M., et al. 2019, ApJS, 243, 24
Prochaska, J. X., Weiner, B., Chen, H.-W., Cooksey, K. L., & Mulchaey, J. S. 2011a, ApJS, 193, 28
Prochaska, J. X., Weiner, B., Chen, H.-W., Mulchaey, J., & Cooksey, K. 2011b, ApJ, 740, 91
Rao, S. M., Belfort-Mihalyi, M., Turnshek, D. A., et al. 2011, MNRAS, 416, 1215
Richter, P., Wakker, B. P., Fechner, C., et al. 2016, A&A, 590, A68
Rudie, G. C., Steidel, C. C., Pettini, M., et al. 2019, ApJ, 885, 61
Rudie, G. C., Steidel, C. C., Shapley, A. E., & Pettini, M. 2013, ApJ, 769, 146
Rudie, G. C., Steidel, C. C., Trainor, R. F., et al. 2012, ApJ, 750, 67
Rykoff, E. S., Rozo, E., & Keisler, R. 2015, arXiv:1509.00870
Smailagić, M., Prochaska, J. X., Burchett, J., Zhu, G., & Ménard, B. 2018, ApJ, 867, 106
Steidel, C. C., Bogosavljević, M., Shapley, A. E., et al. 2011, ApJ, 736, 160
Stocke, J. T., Keeney, B. A., Danforth, C. W., et al. 2013, ApJ, 763, 148
Strateva, I., Ivezić, Ž., Knapp, G. R., et al. 2001, AJ, 122, 1861
Taylor, E. N., Hopkins, A. M., Baldry, I. K., et al. 2011, MNRAS, 418, 1587
Tejos, N., Morris, S. L., Finn, C. W., et al. 2014, MNRAS, 437, 2017
Thom, C., Tumlinson, J., Werk, J. K., et al. 2012, ApJL, 758, L41
Tripp, T. M., Lu, L., & Savage, B. D. 1998, ApJ, 508, 200
Trotta, R. 2017, arXiv:1701.01467
Tumlinson, J., Peeples, M. S., & Werk, J. K. 2017, ARA&A, 55, 389
Tumlinson, J., Thom, C., Werk, J. K., et al. 2011, Sci, 334, 948
Tumlinson, J., Thom, C., Werk, J. K., et al. 2013, ApJ, 777, 59
Turner, M. L., Schaye, J., Steidel, C. C., Rudie, G. C., & Strom, A. L. 2014, MNRAS, 445, 794
Turner, M. L., Schaye, J., Steidel, C. C., Rudie, G. C., & Strom, A. L. 2015, MNRAS, 450, 2067
Wakker, B. P., & Savage, B. D. 2009, ApJS, 182, 378
Werk, J. K., Prochaska, J. X., Cantalupo, S., et al. 2016, ApJ, 833, 54
Werk, J. K., Prochaska, J. X., Thom, C., et al. 2012, ApJS, 198, 3
Werk, J. K., Prochaska, J. X., Thom, C., et al. 2013, ApJS, 204, 17
Werk, J. K., Prochaska, J. X., Tumlinson, J., et al. 2014, ApJ, 792, 8
Wilde, M. C., Werk, J. K., Burchett, J. N., et al. 2021, ApJ, 912, 9
Wolfe, A. M., Gawiser, E., & Prochaska, J. X. 2005, ARA&A, 43, 861
Zahedy, F. S., Chen, H.-W., Johnson, S. D., et al. 2019, MNRAS, 484, 2257